Electromagnetics Laboratory Report Series
Espoo, February 2004 REPORT 426

# STUDYING ELECTROMAGNETIC WAVE-GUIDING AND RESONATING DEVICES

Tero Uusitupa

Dissertation for the degree of Doctor of Technology to be presented with due permission of public examination and debate in Auditorium S4 at Helsinki University of Technology on the 19th of March 2004 at 12 o'clock noon.

Helsinki University of Technology
Department of Electrical and Communications Engineering
Electromagnetics Laboratory

Distribution:
Helsinki University of Technology
Electromagnetics Laboratory
P.O. Box 3000
FIN-02015 HUT
Tel. +358 9 451 2264
Fax +358 9 451 2267

ISBN 951-22-7001-3
ISSN 1456-632X

Picaset Oy
Helsinki 2004

**Abstract**

Various electromagnetic wave-guiding and resonating structures are studied. The structures in question are rather complicated and thus, significant part of the used analysis methods are numerical. Numerical field computation is based on finite-difference method (FD) or on finite-difference time-domain method (FDTD). When possible, analytical methods have been used, often in conjunction with numerical computation. Most of the structures, if not all, find real-life applications. Thus, the focus has been much on such issues as fluency of structure design and quickness of analysis.

Firstly, combline-filter structures are investigated. These components are widely used in mobile communication devices, in radio-frequency and microwave regime, for example. A semianalytic analysis method, which is based on multiconductor-transmission-line theory and 2-D numerical field computation via FD method, is found very efficient. Computationally costly 3-D numerical field computation is avoided. This speeds up the design process of combline filters.

Secondly, so-called hard-surface-waveguide components are analytically studied. When approximating the longitudinally corrugated waveguide wall with an ideal hard surface, one can concentrate on the effects caused by the media inside the tube. First waveguide component is filled with uniaxial anisotropic medium. For this structure, which can be used as a polarisation transformer, analytical solutions are found for transmitted and reflected field, and especially for the helicity of the transmitted field. Second waveguide component is filled with gyrotropic medium, which is electrically controllable ferrite in this case. This component can be used as a mode transformer, for example, from TM to TE mode. Analytical solutions are found for reflected and transmitted fields.

Finally, wave-guiding structures based on photonic-bandgap (PBG) material are studied. This kind of periodically inhomogeneous material is also known as photonic crystal (PhC), having the ability to inhibit the propagation of electromagnetic wave inside the crystal. Carefully designed PBG components may find several applications, for example, in the integrated optics. In this thesis, the focus has been on PBG material based on triangular lattice of air holes etched through dielectric background. Further, waveguide bends have been of special interest, partly because they give a chance of realising tight light-channel bends for integrated optics. Various issues related to FDTD analysis and design of PBG structures are discussed. The importance of PBG-component optimisation is demonstrated. Promising results are obtained for extremely tight bends, although radiation losses in real 3-D structures are recognized as a problem. Some basic components, 60 and 120 degree waveguide bends, and a taper, have been designed.

# Contents

**Acknowledgements** **2**

**List of publications** **3**

**Contribution of the author** **4**

**1 Introduction** **5**

**2 On the structures under study** **6**
2.1 Combline-filter devices . . . . . 6
2.2 Hard-surface-waveguide components . . . . . 9
2.3 PBG-waveguide components . . . . . 11

**3 General considerations about component structure modelling** **17**
3.1 Transmission-line model . . . . . 17
3.2 Multimode waveguide and its TL model . . . . . 18
3.3 On the computation of transmission-line parameters . . . . . 20
3.3.1 Computing matrices $\overline{\overline{C}}$ and $\overline{\overline{L}}$ . . . . . 21
3.3.2 Solving the quasi-TEM modes . . . . . 23
3.3.3 Attenuation factors due to conductor losses . . . . . 24
3.4 FDTD shortly . . . . . 25
3.5 Block-by-block circuit model or all at once? . . . . . 26

**4 Summary of publications** **26**

**5 Errata** **32**

**References** **34**

# Acknowledgements

This thesis contains results and discussion on the research that I have done in co-operation with various co-authors, from various organisations. During the research, my position has been in the Electromagnetics Laboratory of the Helsinki University of Technology.

I wish to thank the personnel of the laboratory for help, guidance, and many vivid discussions. Especially I want to thank my tutor Professor Keijo Nikoskinen for his patient support. Further, I thank Docent Ari Viitanen for his guidance in analytical waveguide research, and D.Sc. Kimmo Kärkkäinen for fluent co-operation. For the computer support, I wish to thank Juha Juntunen and Sami Ilvonen.

Filtronic LK Oy (former LK-Products) and VTT Microelectronics/integrated optics group deserve an acknowledgement for broadening my mind beyond the academic world. Especially, I want to thank co-author Jukka Loukkola from "LK".

For the financial support I wish to thank the Graduate School in Electronics, Telecommunications and Automation (GETA), and LK Products. Finally, I thank my parents, and my friends, who have encouraged me to develop myself.

# List of publications

[P1] T. Uusitupa, J. Loukkola, "Application of multiconductor transmission-line theory to combline filter design", *Microwave and Optical Technology Letters,* vol. 27, no. 2, Oct. 2000, pp. 113-118.

[P2] A.J. Viitanen, T.M. Uusitupa, "Fields in anisotropic hard-surface waveguide with application to polarisation transformer", *IEE Proceedings, Microwaves, Antennas and Propagation,* vol. 148, no. 5, Oct. 2001, pp. 313-317.

[P3] T.M. Uusitupa, A.J. Viitanen, "Mode transformer for hard-surface waveguides", *Conf. Proc. of 31st European Microwave Conference*, vol. 1, EuMC 2001, London, Sept. 24-27, 2001, pp. 141-144.

[P4] T.M. Uusitupa, A.J. Viitanen, "Analysis of finite-length gyrotropic hard-surface waveguide", *Radio Science,* vol. 38, no. 2, 1026, doi:10.1029/2002RS002706, Apr. 2003.

[P5] T. Uusitupa, K. Kärkkäinen, K. Nikoskinen, "Studying 120° PBG waveguide bend using FDTD", *Microwave and Optical Technology Letters*, vol. 39, no. 4, Nov. 2003, pp. 326-333.

[P6] S. Yliniemi, T. Aalto, P. Heimala, P. Pekko, K. Jefimovs, J. Simonen, T. Uusitupa, "Fabrication of photonic crystal waveguide elements on SOI", *Proceedings of SPIE Photonics Fabrication Europe Conference*, vol. 4944, Brugge, Belgium, 28 Oct – 1 Nov, 2002.

# Contribution of the author

[P1] In practice, the author wrote the whole article. The guideline of Section 5 was given by M.Sc. Jukka Loukkola, who also computed the HFSS result. In the article, a finite-difference-method program is used to compute the capacitance matrices $\overline{\overline{C}}_0$ and $\overline{\overline{C}}$, which are the essential parameters of an MTL geometry. This program (C language) has been developed by the author during 1995-1998. Author has also given a talk about the same subject at 27th EuMC [1].

[P2] The idea came from D.Sc. Ari Viitanen, who also originally performed major part of the analysis. The analysis was checked by the author, who also gave some comments about the manuscript and assisted finalising the paper. Related to the subject of this paper, the author gave a talk at MIOP 2001 [2].

[P3] The paper resulted from the collaboration between the authors. Ari Viitanen gave the idea and the guideline of the analysis. The author went through the analysis and finalised the paper. The author gave a poster presentation.

[P4] The starting idea came from Ari Viitanen. Most of the analysis was performed by the author, who also wrote major part of the paper. Matlab codes were developed by the author. During the work, D.Sc. Viitanen gave fruitful comments.

[P5] The author wrote the whole article. The Matlab functions, related to the pre- and post-processing, were written by the author. The FDTD program (C language) used in the field computation has been coded by D.Sc. Kimmo Kärkkäinen. Prof. Keijo Nikoskinen gave some fruitful comments on the manuscript. Related to the subject, the author has given a poster presentation at Bian2000 [3].

[P6] Using the methods described in paper [P5], the author designed all the PBG-waveguide components, i.e., the tapering section, 60° bend, and 120° bend. Author gave guidelines for Section 2 (Component design and modelling) of the article.

# 1 Introduction

It is known that the behaviour of electromagnetic fields is governed by Maxwell's equations

$$\nabla \times \mathbf{E} = -\frac{\partial \mathbf{B}}{\partial t} \tag{1}$$

$$\nabla \times \mathbf{H} = \frac{\partial \mathbf{D}}{\partial t} + \mathbf{J} \tag{2}$$

$$\nabla \cdot \mathbf{D} = \varrho \tag{3}$$

$$\nabla \cdot \mathbf{B} = 0 \tag{4}$$

where the electric field $\mathbf{E}$, magnetic field $\mathbf{H}$, electric flux density $\mathbf{D}$, and magnetic flux density $\mathbf{B}$ all depend on time and location. The field sources are current density $\mathbf{J}$ and charge density $\varrho$. The macroscopic model for the medium can be presented by the so-called constitutive relations. If the medium does not couple the electric and magnetic fields, e.g. via chirality [4], the constitutive relations are

$$\mathbf{D} = \overline{\overline{\epsilon}} \cdot \mathbf{E} \tag{5}$$

$$\mathbf{B} = \overline{\overline{\mu}} \cdot \mathbf{H} \tag{6}$$

where $\overline{\overline{\epsilon}}$ is the permittivity and $\overline{\overline{\mu}}$ is the permeability. All the media within this thesis are such that (5) and (6) are adequate. In some cases the medium is isotropic, i.e., the dyadics $\overline{\overline{\epsilon}}$ and $\overline{\overline{\mu}}$ can be replaced by scalars $\epsilon$ and $\mu$. In some cases material parameters depend on frequency. In every studied case the medium is inhomogeneous, i.e., the material parameters depend on the location in space.

Maxwell's equations predict that electromagnetic waves exist. If inhomogeneous material is somehow - naturally or artificially - regularly arranged, an EM wave can be guided along a certain route. For example, an EM wave can travel along the Earths curved surface, or along a curved plastic rod, or along a coiled TV cable that lies around the floor. If a structure becomes fairly isolated from the outside world, with certain frequencies the structure may become a resonator: in resonance its ability to collect EM energy is remarkably increased. One natural resonator is the Earth with its ionosphere, i.e., the resonator is between two well-conductive spherical surfaces [1]. On the other hand, one artificial resonator is a metal box. Our current civilisation is highly based on artificial wave-guiding structures such as power lines, coaxial cables, and optical fibers. Thus, obviously, research and design of electromagnetic wave-guiding and resonating components has become an important field in modern engineering.

Although nowadays numerical analysis of electromagnetic problems becomes more and more powerful, due to the computer development, analytical treatment and closed-form formulas have their important benefits. Closed-form formulas and symbolic computation give a lot of information in a compact, human-readable form. Analytical solutions can be used to check whether a numerical algorithm works or not. If modelling a very complex system, e.g. a microwave circuit, brute-force numerical field computation is probably ineffective. Known analytical solutions can be

[1] So-called Schumann resonances can be observed in the noise spectrum of the atmosphere. The lowest observed frequency is about 8 Hz with Q value less than 10 [5, pp.272-274].

used with numerics so that the computation cost is remarkably reduced. Fundamental analytical solutions can be found from e.g. [5], [6], [7], and [8]. Each one of these books discusses of electromagnetic theory, waveguides, and resonators. Dielectric waveguides are considered in e.g. [9] and [10].

Numerical field computation has its benefits, too. Very complicated geometries, having inhomogeneous medium, can be studied. A confirmed numerical algorithm can be used to check whether an analytical solution works or not. There is also some educational benefit. For example, if one is using a computer program in dynamic electromagnetic field simulation with a graphical output, one is able to *see* physical phenomena that can not be seen in reality (but that exist). This may grow the intuitive comprehension of EM field behaviour. Sensibly utilised intuition may e.g. help guessing a usable approximative solution or semianalytic model. One problem with brute-force numerical computation is that it can produce a huge amount of data. Picking up, processing, and storing the relevant information can be cumbersome. Setting up a "virtual measurement laboratory" can take a long time.

In this thesis the focus is on certain wave-guiding and resonating electromagnetic structures. The studying methods are partly numerical and partly analytical. The treatment in many cases could be classified as application oriented. In section 2 the studied structures are introduced. After that, in section 3, EM structure modelling issues are considered. Summary of publications is given in section 4.

# 2 On the structures under study

## 2.1 Combline-filter devices

Schematic Figure 1 illuminates a combline-filter structure. The filter operation is es-

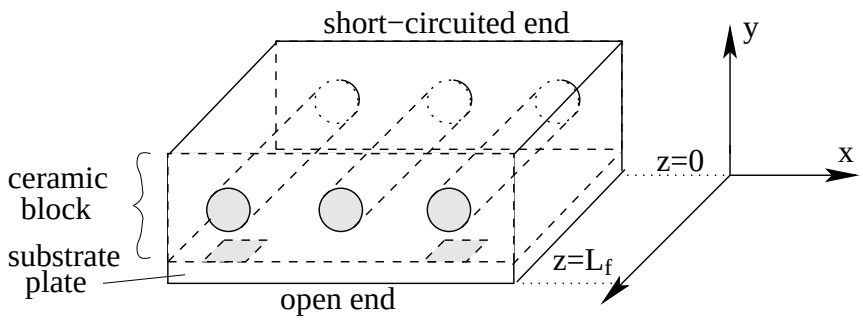


Figure 1: Schematic illustration of a combline filter. Three cylindrical conductors are inside a conductive box, whose one end is left open (not metallised). Inside the box the medium is inhomogeneous. At the short-circuited end $z = 0$, the inner conductors are connected to the conductive box, i.e., to the outer conductor. By the open end, input and output pads (microstrips) are shown. This structure resembles a ceramic combline filter. In practice, $\epsilon_{\text{ceramic}} >> \epsilon_{\text{substrate}}$.

sentially based on quasi-TEM-mode $\lambda/4$ resonances (standing waves in $z$-direction) and thus, crucial physical parameters are the length of the conductors $L_f$ and the medium parameters $\epsilon$ and $\mu$. Abbreviation TEM stands for transverse electromagnetic, i.e., in this case field vectors are mainly in $xy$-plane. In the shown structure

material is inhomogeneous, i.e., $\epsilon$ and $\mu$ are not constant. In practice though, traditionally $\mu$ has been $\mu_0 = 4\pi \cdot 10^{-7}$ Vs/Am.

Combline filters are often used in mobile communication devices. In a cellular phone, a so-called duplexer component that is handling received and transmitted signal, can be realised using combline filters. Using high-permittivity material as the medium surrounding the inner conductors, shrinks the wavelength, and thus makes the filter component small [2]. There exist low-loss high-permittivity ceramic materials. Thus, *ceramic* combline filters have been widely used in handsets. In short, a ceramic filter can be roughly thought as a $\lambda/4$ long multiconductor-transmission-line (MTL) resonator, whose one end has been short-circuited. In a real filter component, combined with this MTL resonator structure, also some microstrip elements are used, such as input/output pads and strip lines to control the filter response. These elements lie on the substrate plate, which is situated under the ceramic block (Figure 1). Often in a real duplexer component, the receiving and transmitting filter, both connected to the antenna, are situated side by side in the same ceramic block. The receiving and transmitting filters have a bit different length, because their pass bands must be centered at different frequencies.

In base-station use, the combline filters are often air-filled, and thus, their physical size and power-handling capacity is substantially higher compared to ceramic filters. Also in these components, the pure combline structure is enhanced by some additional parts. For example, tuning screws are used at the open end, to control the fringing-field load capacitances, which affect the filter response.

Combline filters have been widely used in personal radio communication devices (walkie-talkies, mobile phones). The frequency range of use has traditionally been in the RF and lower microwave regime, i.e., within UHF where $f = 300 - 3000$ MHz [11], [10]. Within this frequency range the quasi-TEM-mode conductor losses are still acceptable, if good conductive material is used, such as silver or copper [3]. If the conductors are poor or the frequency is too high, loss power becomes too high. In that case the quality factor $Q$ of the resonator filter decreases, and in general, a significant part of the inputted electrical power transforms to heat.

Considering this thesis, in paper [P1] combline-filter structures have been studied. The basic assumption has been that the frequency is low enough in order to allow only the propagation of quasi-TEM modes [12]. Thus, the used method has a better chance to work, if the frequency range of analysis is below the cut-off frequencies of the higher modes. For example, if the radii of the inner conductors shrink to zero, the cut-off frequency of the first higher mode ($\mathrm{TE_{z10}}$) is

$$f_{\mathrm{c10}} = \frac{c_0}{2w_f\sqrt{\epsilon_r}}, \tag{7}$$

where $w_f$ is the filter width in $x$-direction, $c_0$ is the speed of light in vacuum, and material is assumed homogeneous with relative permittivity $\epsilon_r$. With nonzero radii of the inner conductors, the filter box becomes effectively smaller, fortunately, causing the higher mode $f_c$ to increase from the value given by (7). In paper [P1], the numerical example was computed for a structure with $w_f = 5$ mm, ceramic block having $\epsilon_r = 82.3$ and substrate $\epsilon_r = 3.5$. Simply assuming the material entirely

[2] This is probably one of the reasons why the cellular phones are so small nowadays.

[3] It is known that TEM-mode conductor loss power depends on the factor $\sqrt{f/\sigma}$ [5],[6].

ceramic (thin substrate), from (7) one gets $f_c = 3.3$ GHz. The message is that a mode resembling $\mathrm{TE}_{z10}$ can not propagate in the example case within the frequency range of analysis. With certain real ceramic-filter structures $w_f$ might get too high, in which case the method, at least theoretically, becomes a bit suspicious. With these kind of "wide structures", the obtained filter response may lack some features that should exist.

Assuming that only quasi-TEM modes propagate, a MTL model has been used. Utilising MTL model requires solving the phase velocities $v_i$ for each quasi-TEM mode, $i = 1...n$, where $n$ is the number of inner conductors. Propagation factors are $\beta_i = \omega/v_i$. Also, the voltage eigenvectors $\overline{V}_i$ and current eigenvectors $\overline{I}_i$ on the conductors must be solved, for each mode. The quantities $v_i$, $\overline{V}_i$, and $\overline{I}_i$, $i = 1...n$, can be solved, if the capacitance matrix $\overline{\overline{C}}$ and inductance matrix $\overline{\overline{L}}$ are known for the MTL cross-sectional geometry. These matrices, $\overline{\overline{C}}$ and $\overline{\overline{L}}$, have been computed numerically via solving potential distributions by finite-difference method (see Section 3.3). Paper [P1] also discusses computation of mode attenuation factors $\alpha_i$ and computation of MTL discontinuity fringing-field capacitances [4]. By including $\alpha_i$'s and some extra discontinuity capacitances into the circuit model, one could expect to obtain a more accurate model. However, firstly, extraction of these parameters requires additional numerical computation. Secondly, these parameters are not as relevant as $\overline{\overline{C}}$ and $\overline{\overline{L}}$. Thus in practice, with ceramic filters, it may be sensible to limit the numerical parameter extraction to $\overline{\overline{C}}$ and $\overline{\overline{L}}$ computation.

Let us shortly concentrate on the filter structure shown in paper [P1], Figure 3, and consider some principles how the filter response is determined. If neglecting parasitic effects, such as the open-end capacitances, the lowest pass band is situated around the quasi-TEM-mode resonance frequencies. In this case there is two cylindrical conductors symmetrically situated, i.e., the propagation modes are even and odd. Even-mode voltages are similar to (1 1) V, and odd-mode voltages are similar to (1 -1) V. The inhomogeneous medium causes that $\beta_{\mathrm{even}} \neq \beta_{\mathrm{odd}}$. With the ceramic filter considered here, $\beta_{\mathrm{odd}} > \beta_{\mathrm{even}}$, because odd-mode field experiences a higher effective permittivity, $\epsilon_{\mathrm{odd}} > \epsilon_{\mathrm{even}}$. The pass band is around $\lambda/4$ resonances, which are now

$$f_{\mathrm{odd}} = \frac{c_0}{4L_f\sqrt{\epsilon_{\mathrm{r,odd}}}} \ , \qquad f_{\mathrm{even}} = \frac{c_0}{4L_f\sqrt{\epsilon_{\mathrm{r,even}}}} \ . \tag{8}$$

If the distance between the conductors is increased, or, if the contrast between the medium permittivities is decreased, the effective permittivities $\epsilon_{\mathrm{odd}}$ and $\epsilon_{\mathrm{even}}$ get closer to each other. Thus, also $\beta$'s and resonances become closer to each other.

If the resonator is almost lossless and the connection to the outside world is weak, the quality factor $Q$ of the structure is high. Thus, the resonance peaks are narrow. In this case, in the filter response $|S_{21}(f)|$, there is no proper pass band. Instead of a flat pass band, one observes twin peaks, caused by the two resonances. Increasing the coupling to the outside world makes the peaks wider and flattens the pass band. The coupling can be affected by the metal strips on the substrate (input-output

[4] The author has written C programs for $\alpha_i$ computation and for solving a fringing-field capacitance network. Both programs are partly based on finite-difference method (FD). Computation of fringing-field capacitances $c^f_{ij}$ requires 3-D FD. Thus, computing $c^f_{ij}$ can be relatively time-consuming.

pads). If keeping other dimensions constant, increasing the strip length makes the coupling stronger. It is easy to understand, via a capacitance model, that making the strips e.g. very short, dramatically drops the coupling.

Real ceramic-filter structures usually have more than two cylindrical conductors. For example, with five conductors there is five quasi-TEM modes and thus, five quasi-TEM resonances, which affect the filter response. In practice, the microstrip configuration on the substrate causes that the structure is not uniform in $z$-direction. To some extent, this can be taken into account by cascading MTL's, each MTL corresponding to a bit different cross-sectional geometry. Of course, the usability of the MTL-based model is higher with highly-uniform structures (e.g. only two or three MTL's cascaded), and with low frequencies.

## 2.2 Hard-surface-waveguide components

In the microwave regime, roughly around $f = 1 - 30$ GHz, metal-tube waveguides become suitable, especially when high electromagnetic power must be transferred. Also, considering electromagnetic compatibility, these kind of closed structures are convenient: metal-tube waveguides do not radiate power sidewards, and also, the field is zero outside the tube walls [5]. Of course, an *open end* of a metal tube can radiate, i.e., act as an aperture antenna.

In some applications, such as reflector-antenna horn feeds, the inner flat metal wall of the waveguide is replaced by a corrugated metal surface (Figure 2). For

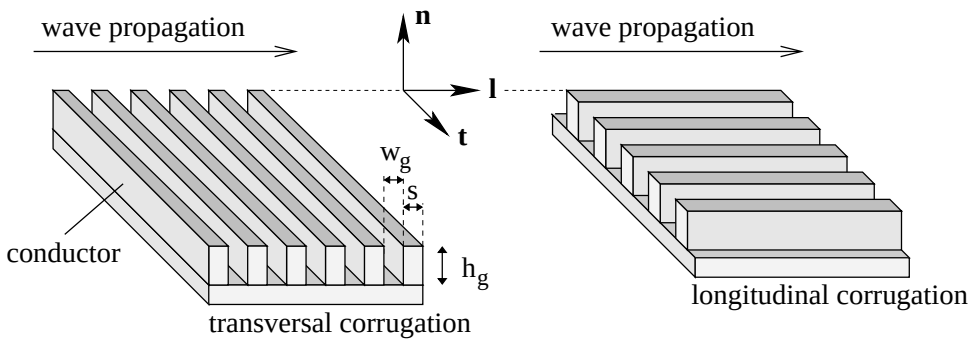


Figure 2: Corrugated surface. Axes $n$, $l$, and $t$ stand for normal, longitudinal, and transversal directions, respectively.

example, with a transversely corrugated circular horn antenna it is possible to obtain an aperture field of type $\mathbf{E} \propto J_0(K\rho)\mathbf{u}_x$, where $J_0$ is the Bessel function of first kind, $K$ is the transverse wavenumber, and the symbol $\propto$ denotes "proportional to". So - in ideal case the electric field lines are straight in the aperture ($\mathbf{u}_x$) and the field strength is circularly symmetric (no $\varphi$ dependency). Thus, in practice, very low cross-polarisation in radiated field is obtained and also the radiation pattern is circularly symmetric [13, pp.7 – 9].

A corrugated surface is made up of parallel grooves, separated by metal walls. The boundary condition is applied at the surface that lies on the wall tops, i.e., at

[5] For comparison, if a dielectric slab is used as a non-radiating waveguide, the field does spread outside the structure.

$n = 0$. Let $k_n$ be the wavenumber in depth direction inside the groove. If the depth of the grooves $h_g$ is such that $k_n h_g = \pi/2$ and the corrugation is dense enough, the boundary conditions for electric field are approximately [14]

$$E_t = 0, \quad E_n = 0 \quad \text{(transversal corrugation)} \tag{9}$$

$$\frac{\partial E_t}{\partial n} = 0, \quad \frac{\partial E_n}{\partial n} = 0 \quad \text{(longitudinal corrugation)} \tag{10}$$

These approximations hold better the smaller the period $w_g + s$ is compared to the wavelength $\lambda$. It has been defined so that transversal corrugation implies *soft surface* (SS) and longitudinal corrugation implies *hard surface* (HS). The background of these definitions is in acoustics [6].

The boundary condition depends on the electrical depth $k_n h_g$ of the grooves, making the boundary frequency dependent. For example, with hard surface, for transverse electric field inside the groove one can write

$$E_t \propto \sin[k_n(n + h_g)]e^{-j\beta l}, \tag{11}$$

assuming that wave propagates in $+l$-direction. Condition $k_n h_g = \pi/2$ stands for $\lambda/4$ resonance: at $n = -h_g$ $E_t = 0$, and at $n = 0$ $E_t$ has its maximum i.e. $\frac{\partial E_t}{\partial n} = 0$. In order to decrease the physical groove depth, usually the groove is filled with dielectric material having $\mu = \mu_0$, $\epsilon = \epsilon_g$. Further, the higher the permittivity $\epsilon_g$ is, the less $k_n = \sqrt{\omega^2 \mu_0 \epsilon_g - \beta^2}$ depends on the propagation factor $\beta$ in the waveguide.

In this thesis, circular hard-surface waveguides filled with different media have been studied. In paper [P2] uniaxially anisotropic dielectric is used, and in papers [P3] and [P4] electrically controllable ferrite is used. The $\lambda/4$ resonance condition has been assumed, i.e., corrugation implies hard surface. Thus, for longitudinal electric and magnetic field it holds:

$$E_l = 0, \quad H_l = 0 \quad \text{on the HS boundary.} \tag{12}$$

This convenient boundary condition is appropriate, if the frequency $f$ is such that $k_n h_g \approx \pi/2$, and the corrugation is dense ($w_g + s << \lambda$). If $f$ is somewhat deviated from the resonance, assumption $E_l = 0$ is still acceptable, but assumption $H_l = 0$ is not, because boundary condition for $H_l$ depends on the electrical depth $k_n h_g$, i.e., in the groove

$$H_l \propto \cos[k_n(n + h_g)]e^{-j\beta l}. \tag{13}$$

So - if $f$ is out of the $\lambda/4$ resonance, condition (12) does not hold exactly. Nevertheless, pure TE and TM modes can still propagate [15, pp. 183 – 185], even if the field has $\varphi$ dependency. But, because the out-of-resonance boundary condition is something like $E_l \approx 0, H_l \neq 0$, TM and TE field can not have exactly same $(\rho, \varphi)$ dependency.

[6] In acoustics, on soft surface, the sound pressure $p = 0$. On hard surface the normal derivative $dp/dn = 0$. Thus, associating $p$ with electric field components $E_t$ and $E_n$, one can talk about electromagnetic soft and hard surface. The condition for the longitudinal field component is not as relevant, if considering power propagation along the surface.

Using simple boundary condition (12) in the analysis, one can effectively concentrate on the effects of the medium inside the HS waveguide. Hard-surface waveguide filled with anisotropic dielectric material was studied in [P2]. Anisotropic waveguide section between isotropic sections can be used as a polarisation transformer. E.g, the polarisation state of the field can be changed from linear close to circular. The device operation is based on different propagation constants of TM and TE mode fields, i.e., on the phase-shift difference $(\beta^{\mathrm{TM}} - \beta^{\mathrm{TE}})d$, where $d$ is the length of the anisotropic waveguide. For example, if in the incident field TM and TE components oscillate in the same phase, the field is linearly polarised. If after the anisotropic section the phase-shift difference is 90°, the TM and TE components oscillate so that the resultant field is elliptically polarised. Obviously, the polarisation transformation requires that the incident field is hybrid, i.e., containing TM and TE part.

In papers [P3] and [P4] hard-surface waveguide filled with ferrite was studied. Ferrite is electrically controllable gyrotropic medium, i.e., the medium properties can be changed by electric current. For example, the ferrite rod can be put inside a current coil. Gyrotropic waveguide section between isotropic sections works as a mode converter, e.g., from TM to TE field. The orientation of the **E** and **H** fields is changed as the wave propagates along the gyrotropic WG (waveguide). Mode conversion results from the fact that instead of TM and TE, the eigenfields in the gyrotropic waveguide are hybrid mode fields, named as plus and minus fields. With nonzero gyrotropy parameter $\mu_g$, $\beta^+ \neq \beta^-$. The phase-shift difference $(\beta^- - \beta^+)d$ causes the mode conversion.

## 2.3 PBG-waveguide components

Photonic-band-gap (PBG) material, or photonic crystal, is *periodically* inhomogeneous material, which prevents propagation of electromagnetic waves in the band-gap frequency range (stop band). Thus, properly fabricated PBG material can be used as frequency-selective reflective medium. Potential applications are highly efficient optical lasers and sharp bends in optical waveguides, for example. No metal is needed to obtain total reflection. In some cases this might make a component cheap and lightweight. So, considering total reflection, purely dielectric material may be sufficient, as long as the material is periodic, i.e., forming a regular lattice. Two example lattices are shown in Figure 3. A physical implementation could be e.g. a silicon plate having vertically etched holes.

The word "photonic" is a bit misleading, because PBG's can be utilised in all frequency ranges. Thus, quite often an abbreviation EBG (Electromagnetic Band Gap) has been adopted. The frequency range of stop-band operation essentially depends on the lattice constant $a$, the distance between the lattice elements. For example, with optical frequencies the lattice constant has to be roughly around 0.1–1 $\mu$m, and with $f \approx 1$ GHz $a$ is around 3–30 cm. The exact frequency range of PBG operation depends on many other physical parameters, too, such as media parameters, lattice type, and lattice element geometry. In [16] so-called gap maps are given for certain lattices. From a gap map one can see how the stop-band locations and widths depend on certain lattice parameters, such as $d/a$ or dielectric contrast. Briefly, a PBG waveguide can be realised by making a linear lattice defect in the

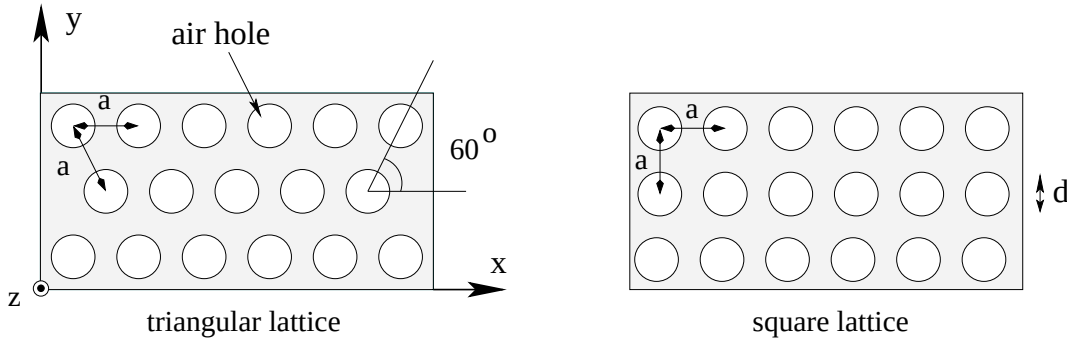


Figure 3: Examples of 2-D PBG lattices. 2-D refers to two-dimensional and means that the structure is assumed uniform in $z$-direction. If frequency is within the band gap, the wave can not propagate in the lattice in $xy$-plane.

PBG material. When the regular lattice consists of air holes, linear defect means that holes are not processed along a line (Figure 4). If only one hole is missing, it is

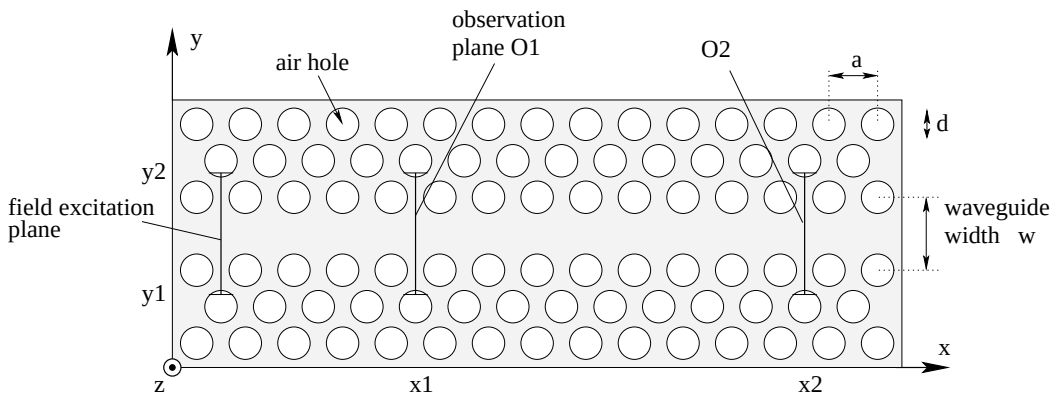


Figure 4: Straight PBG waveguide with some notations. If the excitation field distribution and frequency are properly chosen, the field starts to propagate from the excitation plane, along the waveguide in $x$-direction, towards the observation planes O1 and O2.

often called as a point defect. A point defect may act as a micro-cavity resonator, for example.

Of course, a real PBG waveguide (PBG-WG) has a 3-D geometry. Figure 5 shows an example of a PBG-WG cross-section. The thickness of the PBG plate affects on the amount of radiation losses and on the effective refraction index $n_{\text{eff}}$ seen by the wave (propagating now in $x$-direction). If the thickness grows, radiation is reduced and also, $n_{\text{eff}}$ becomes less dependent on the material above and below the plate (SiO2). So, for example - the thicker the PBG plate is, the better a 2-D computation model works (no $z$ dependency).

Next, a short overview is presented about potential PBG applications. In microwave and millimeter wave regime patch antennas have become popular, because they are relatively easy to manufacture and cheap. But because of the substrate surface waves, which can be considered as a loss mechanism, the antenna radiation

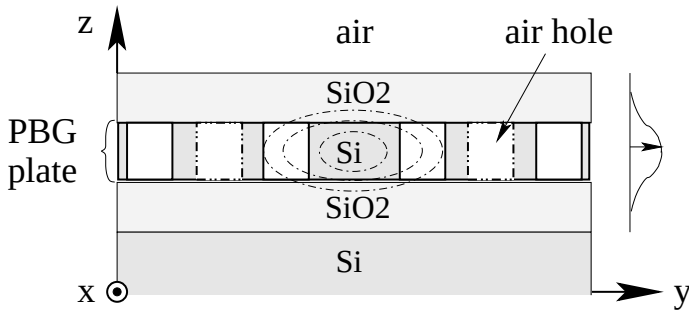


Figure 5: A cross-section of a PBG-WG. The waveguide is formed along the $x$-axis, i.e., the field is meant to propagate in $x$-direction. With a proper excitation, the field will be mostly concentrated in the PBG-plate region, especially in the Si region in the middle, and the radiation losses will be minimised. To be exact, proper excitation means correct positioning and profile of the excitation field, correct time dependency, and correct polarisation. The shown material layering resembles a so-called SOI structure (silicon-on-insulator).

efficiency is degraded. PBG substrate can inhibit the surface waves and thus, increase the radiation efficiency [17]. Another possible application is with microstrip filters. By drilling holes into the ground plane so that the holes are centered under the strip, one can obtain filters having high rejection values and high cut-off sharpness. High rejection level, e.g. $S_{21} < -60$ dB, requires a large number of hole periods along the microstrip line. A compact solution is proposed in [18], where the microstrip line snakes on the PBG ground plane, instead of forming a (long) straight line.

In optical and infrared regime, spontaneous emission is degrading the performance of semiconductor lasers and LEDs. Spontaneous emission, which is usually unwanted radiative recombination of electrons and holes, can be inhibited if the photons can not propagate away from their place of birth. Properly designed PBG structure may stop the photons and increases the efficiency of semiconductor lasers [19].

If considering high-rate and long-link optical communications, photonic-crystal fibers (PCF) or photonic-bandgap fibers (PBGF) may have some useful features. In these structures a lateral PBG is implemented by periodic cladding [20]. Because the operation of these fibers is not based on total internal reflection, the core permittivity can be smaller than the cladding permittivity. Further, because of the quasi-metal boundary, a truly monomode optical fiber may be obtained, i.e., higher modes are cut off in a similar way as in a metal-tube waveguide.

Traditional dielectric waveguides or fiber-optic cables rely on total internal reflection (TIR). However, if a bend in a light-guiding structure is too tight, TIR does not work and consequently, light escapes from the guide. For example, making a 90° bend in a traditional dielectric waveguide, causes that only 30 % of the incident power is transmitted through the bend [21]. Tight bends become necessary in e.g. integrated optics: miniaturisation of optoelectronic components and circuits requires that low-loss tight waveguide bends can be fabricated. Forming a waveguide in a PBG lattice may be the solution. It is possible to have a 90° or even a 120° bend

so that roughly 100 percent of the power is transmitted through the bend (paper [P5]). However, these promising computed results for PBG bends are obtained in 2-D case. Taking also the third dimension into account, i.e. allowing finite PBG-slab thickness, involves upward and downward radiation losses. These losses reduce the transmission. Thus, one future challenge in PBG research is to find solutions to diminish out-of-plane radiation losses.

In sum, one major advantage of PBG is that via radiation control, many components can be made more efficient and less lossy. Second major advantage is that novel components for e.g. optical circuits may be designed.

Let us consider here shortly the nature of a PBG waveguide (Figure 4). For simplicity, assume first an ideal 2-D structure, where the geometry and the fields do not depend on $z$ at all. Two cases are discussed. First, $f$ is within the band gap, and then, $f$ is out of the band gap.

1. If $f$ is within the band-gap range, wave can not propagate in the lattice, which is surrounding the waveguide. Thus, power can not radiate away from the waveguide, i.e., the structure is rather closed. Radiation is inhibited, whatever the field distribution (mode) is inside the waveguide. For comparison, it is well known that in a conventional dielectric WG, the amount of radiation loss does depend on the field distribution. Thus, the PBG-WG structure is similar to a metal tube waveguide. For example, if frequency is too low, under the cut-off frequency of the mode in question, power can not propagate along the PBG waveguide [7].

2. From Figure 6 of paper [P5] it is seen, how strongly the reflectivity of a PBG wall depends on the frequency. A 15 % frequency drop might change the PBG-WG wall reflectivity from 100 % close to zero. Now - if $f$ is no longer within the band gap, the waveguide becomes "open" and power can radiate away. The amount of radiation loss depends on the field distribution of the propagating wave. Also, the type of the lattice matters. If $f$ is relatively low, the WG shown in Figure 4 resembles a dielectric slab WG, where lossless propagation is possible with certain modes, at least with the lowest mode. Low-loss propagation is possible in this case, because along the WG the effective permittivity is *higher* than in the surrounding lattice. However, if the PBG-WG was based on a linear defect in a lattice of dielectric rods in air, the WG structure would be very lossy. Namely, in that case, the effective permittivity in the WG would be *less* than in the lattice surrounding the WG [8].

If the PBG-WG structure, e.g. the one shown in Figure 4, is such that the PBG plate has finite thickness in $z$-direction, there will be upward and downward radiation loss (out-of-$xy$-plane loss), i.e., $\Re\{S_z\} \neq 0$, where $S_z$ is the $z$-component of the Poynting vector. So, a real 3-D waveguide, based on a simple 2-D lattice, is not ideally closed

[7] This holds for a WG having infinite length. In a finite-length WG power can propagate, even if $f$ is below cut-off frequency. The shorter the WG, or, the closer $f$ is to the $f_{\mathrm{cut-off}}$, the better the power propagates.

[8] To be exact, the effective permittivity of the lattice depends on the field polarisation and is thus a dyadic (or matrix).

even if $f$ is within the band gap [9]. In general, the thinner the plate is, or, the stronger the $z$ dependency of the propagating field is, the more there will be radiation loss in $z$-direction (paper [P5]). It is also known that increasing the hole size, e.g. from $d/a = 0.5$ to $d/a = 0.7$, increases the out-of-plane losses [22]. Further, it is easy to believe that the etch depth of the holes has an effect, too. Incompletely etched holes cause higher losses than holes etched all the way through the PBG plate [23].

Now - let us see an example case that illuminates the nature of a PBG-WG bend. For simplicity, a 2-D geometry is assumed. A 60° bend is formed in a triangular lattice of air holes (Figure 6). Background medium has $\epsilon_r = 12.11$, relative hole size is $d/a = 0.76$. Thus, the $\mathrm{TE}_z$ band gap takes effect between $fa/c = 0.235...0.37$ [24], where $c$ is the speed of light in vacuum. Inside this band, there is a chance to have a non-radiating PBG-WG for $\mathrm{TE}_z$ polarisation, i.e., a functional PBG-WG bend. At the bend, there is a small extra hole ($d/a = 0.5$), whose position is varied in the direction of the shown arrow. This variation will affect the bend transmission spectrum, as shown in Figure 6 (right), where two power-flow spectra are shown. It is seen that seemingly small change in the position of the extra hole can

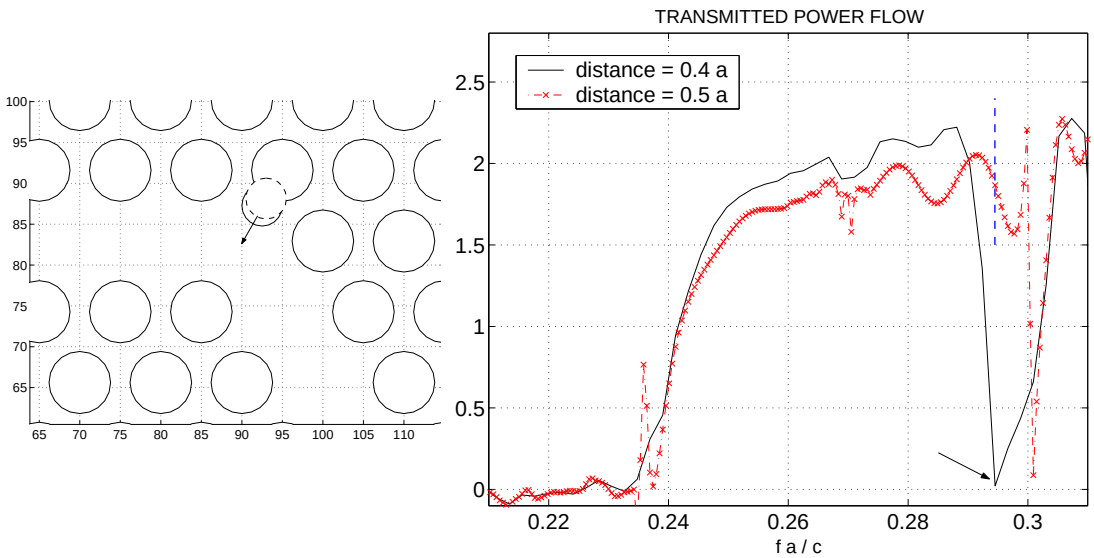


Figure 6: Left: 60° bend with a small extra hole (a zoomed view). The distance of the extra hole from the bigger hole is varied. Distance is measured between the circle centres. The shown two small circles are in distances $0.4a$ and $0.5a$ from the bigger hole. Right: Power-flow spectra, computed just after the bend. Changing the distance from $0.4a$ to $0.5a$ alters the spectrum of transmitted power.

clearly change the power-transmission spectrum. Considering PBG-WG fabrication for optical regime, this result suggests that good quality manufacturing process is required at central locations of the structure. Fortunately in practice, it seems to be so that the hole locations *can* be set very accurately (paper [P6]). But if there is error in the effective hole size, due to non-uniform vertical etch profile, for example,

[9] But of course, it should be possible to design a 3-D PBG-WG having negligible radiation loss. However, this may require adopting PBG reflector in all directions. Thus, the structure may be difficult to manufacture, compared to silicon plate with a hole pattern.

that might affect on the power transmission [10].

At the fixed frequency $fa/c = 0.2945$, the bend seems to have some switch-like behaviour. Transmitted power depends strongly on the position of the extra hole. One may ask, what can cause this behaviour. Figure 7 may give the answer. Two $H_z$-field snapshots are shown. The left one corresponds to extra-hole distance $0.4a$, and the right one to $0.5a$. In both cases, the excitation has been by the left edge of the structure, and, in both cases, the input signal has been a long modulated Gaussian pulse, with modulation frequency $fa/c = 0.2945$. Figure 7

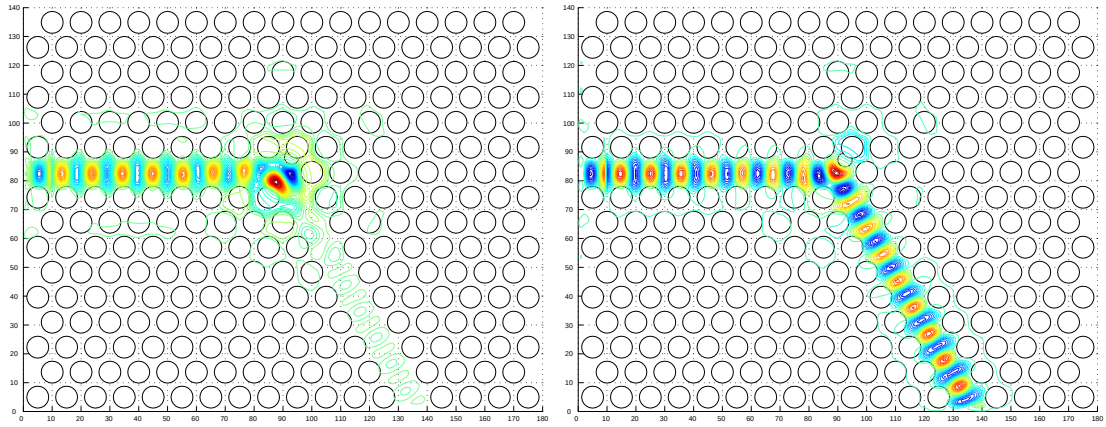

Figure 7: $H_z$-field snapshots. Extra-hole distance is $0.4a$ (left) and $0.5a$ (right).

suggests that the position of the extra hole determines, how much antisymmetric mode is generated at the bend. However, antisymmetric mode can not propagate at this frequency, i.e., the frequency is too low (cut-off condition for antisymmetric mode). Thus, the more antisymmetric mode is generated, the less the bend transmits power through. Finally, note that the shown power-flow spectra are normalised: they have been obtained by dividing the transmitted power flow by the (band-limited) power spectrum of the input signal. Hence, the filtering effect due to the structure itself is obtained.

In this thesis the focus has been on dielectric PBG structures based on triangular lattice of air holes. Further, usually $\mathrm{TE}_z$ polarisation has been assumed, although research has also been done with $\mathrm{TM}_z$ polarisation. Originally, one reason for choosing the triangular lattice was the possibility to have a band gap for $\mathrm{TE}_z$ and $\mathrm{TM}_z$ polarisations within the same frequency range [16]. With this possibility, there is a chance to obtain a light-polarisation-independent PBG component. Another reason was that this kind of lattice suits well for optics and for the used fabrication process (see paper [P6]). Namely, the work has been related to a project, where one objective has been to test fabrication of real PBG components for infrared regime. Also, the promising and interesting nature of the PBG phenomenon has been a motivation for the studies.

The work related to papers [P5] and [P6] involves quite much numerical computation and handling data flow. In paper [P5] various issues related to simulation arrangements and PBG-WG-component design are discussed. In practice, component design involves optimisation. One optimisation cycle can be formally divided

[10] In a real 3-D PBG-WG, non-uniform vertical etch profile may also add radiation losses.

to pre-processing, simulation, and post-processing. In this work, the simulation of the electromagnetic fields has been done using a non-commercial FDTD program STEPS [11]. The pre-processing and the post-processing have been implemented by various Matlab functions and scripts. The PBG-component research is further discussed in summary of papers [P5] and [P6].

# 3 General considerations about component structure modelling

Major part of the studies performed can be considered as application oriented: the studies are related to component design and modelling issues. Thus, a crucial issue is the effectiveness of a modelling method. For example, along an optimisation process, it is convenient to obtain sensible modelling results as quickly as possible.

## 3.1 Transmission-line model

Figure 8 shows a section of transmission line (TL), having impedance $Z$ and propagation factor $\beta$. Theory of TL's can be found in e.g. [5], [26], [27], [6], [7], and [8].

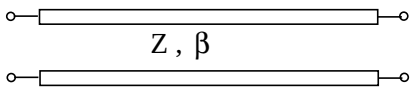


Figure 8: Transmission line.

If the salient features of a physical electromagnetic structure can be modelled by transmission lines, the modelling process can be very effective. The reason is that by using TL theory less numerical computation is needed. For example, in paper [P1], a complicated 3-D ceramic-filter structure is simulated using a circuit simulator with TL model, thus, avoiding computationally costly 3-D field simulation.

Briefly, TL model is convenient with uniform wave-guiding structures, which have a constant cross-sectional geometry. Using TL model requires solving the TL parameters $Z$ and $\beta$ of the analysed propagation mode. With some geometries this can be done analytically. For example, analytical solutions are known for rectangular and circular waveguide, and for some TEM waveguides, e.g., coaxial cable and two-wire line. But in general case, one has to use approximative formulas, or compute the parameter values numerically.

Further, individual uniform waveguide sections, each having a different $Z$ and $\beta$, can be cascaded, and the chain of waveguides can be analysed using TL theory. For example, if a circular waveguide has a perpendicular interface of an air-filled and dielectric-filled sections, the reflection and transmission of a certain TM or TE mode can be analytically solved.

[11] STEPS has been developed in the Electromagnetics laboratory by D.Sc. Kimmo Kärkkäinen. The author has taken part in the developing process by testing the program extensively. STEPS has been used by the author also with multimode resonator studies in microwave regime [25].

In general, when using TL theory to study waveguide discontinuities, one has to require that the field profile is same at the both sides of the interface, e.g., $TE_{10}$ field of a rectangular waveguide. Namely, even if the geometry and dimensions of *individual* waveguides can be modelled via $Z$ and $\beta$, the physical consequences of a *geometrical discontinuity* are not properly modelled by simply cascading two transmission lines. For example, if in a circular waveguide a fundamental-mode field is coming to an interface, where the tube diameter suddenly increases, new modes are generated. Some of them propagate power, some of them are evanescent. Anyway, these new modes caused by the discontinuity are not taken into account in a simple TL model, where one assumes only one mode per waveguide.

Discontinuity in the cross-sectional geometry does not always destroy the idea of using simple TL model. Often with quasi-TEM waveguides TL model gives usable results. For example, with a structure consisting of two cascaded microstrip lines, having strip widths $w_1$ and $w_2$, one can assume a quasi-TEM mode propagating at both sides of the discontinuity, if $f$ is not too high. Sensible results for reflection and transmission are obtained, especially if discrete components are included at the interface to model local field effects caused by the discontinuity. In the case of an abrupt change in microstrip width, current compression can be modelled via a series inductance and the fringing electric field via a parallel capacitance [28], [29], [30]. Also with a dielectric-slab-waveguide discontinuity, simple TL model can give usable results. Assume a structure consisting of two cascaded dielectric WG's, having widths $w_1$ and $w_2$. If the step discontinuity is small enough, and if at the both sides monomode propagation can be assumed, the main effect of the step is a change of impedance [10, pp. 189–191]. E.g., reflection coefficient is simply $(Z_2 - Z_1)/(Z_2 + Z_1)$, where the impedance values are solvable without numerical field analysis for e.g. dielectric-slab WG's.

Obviously, the TL model shown in Figure 8 suits only for a single-mode waveguide. Many structures require a model for multimode propagation, such as the waveguide components studied in [P1] and [P2].

## 3.2 Multimode waveguide and its TL model

In this thesis, many of the studied structures have the following nature:

- structure can be considered as a cascade of different waveguides
- in each waveguide there can be many modes propagating

A waveguide supporting multimode propagation can be modelled so that there is a separate transmission line for each mode (Figure 9). These lines can be considered separate, i.e., there is no coupling between them, if the waveguide modes are power orthogonal [12].

[12] Modes are usually defined so that they are power orthogonal to each other. In practice, it may occur that power-orthogonal modes of an ideal waveguide are not exactly power orthogonal in a non-ideal waveguide. For example, in a non-ideal waveguide with surface resistance $R_s = \sqrt{\omega\mu/2\sigma} \neq 0$, a TM mode may couple power to a TE mode, and vice versa. In a circular waveguide with a rotationally symmetric mode (no $\varphi$ dependency), this coupling is avoided [5, pp. 176–179].

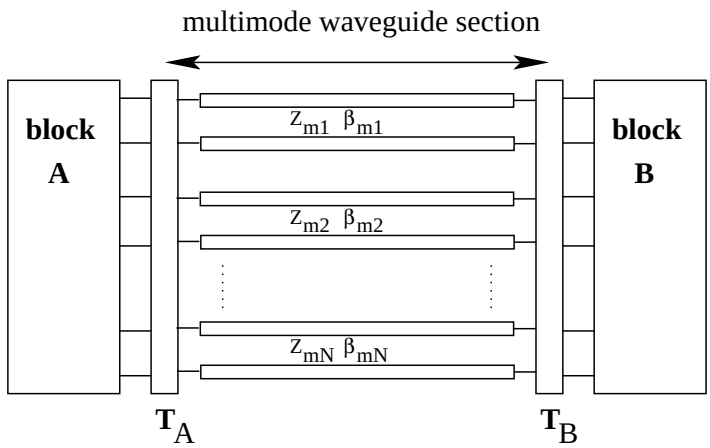


Figure 9: Transmission-line model for a multimode waveguide.

Sometimes using this kind of model requires a change of basis at the interfaces: e.g., the field or circuit quantities from block A must be expressed using the eigenmodes of the multimode waveguide section. Thus, there must be transformation networks $T_A$ and $T_B$ to tell, how strongly e.g. a certain block A mode, incident to the multimode section, is coupled to the different propagation modes. The shown blocks A and B can be other multimode waveguides, or, circuit blocks consisting of discrete electrical components. Obviously, using the model of Figure 9 requires that the relevant propagation modes (i.e. the basis) are known. Often the WG structures are such that, solving these modes has to be done via numerical field computation. Further, the coupling coefficients of different modes must be known at the interfaces, to construct the transformation networks $T_A$ and $T_B$.

In paper [P1] ceramic combline filter is studied assuming that the structure consists of cascaded multiconductor transmission lines. The relevant modes are quasi-TEM modes. Solving these requires numerical field analysis. The simulation of the filter is done in a circuit simulator, which has some built-in functions to model an MTL. In this case, the transformation networks are controlled voltage and current sources, because instead of fields, voltages and currents are simulated.

In paper [P2] anisotropic HS-WG section is situated between isotropic HS-WG's (blocks A and B). Each section is modelled using two transmission lines: there is a separate line for TM and TE mode (Fig.3 in paper [P2]), because these modes can propagate independently from each other. In this case, transformation networks are not required, because in all the waveguide sections fields can be expressed using the same TM-TE basis, and there is no coupling between TM and TE modes at the interfaces.

In paper [P4] gyrotropic HS-WG section is situated between isotropic HS-WG's. In this case, a change of basis is needed, because the eigenmodes in an isotropic HS-WG are TE and TM modes, but in a gyrotropic HS-WG the eigenmodes are plus and minus waves, which are hybrid modes. Actually in the paper, the basis change is embedded in the transmission and reflection coefficients (formulas (71), (72), (86), and (87)). In this paper, the analysis of the interfaces is done by requiring the continuity of the transverse fields, i.e., TL theory is not directly applied to get the reflection and transmission of the cascaded waveguides.

Finally, let us have a very simple example, assuming a symmetric MTL cross-sectional geometry with two inner conductors. Assume block A having a sinusoidal excitation such that the true conductor voltage phasors at the other MTL end, at $z = 0$, are $V_1(0)$ and $V_2(0)$. Assume block B as an absorbing end, or that the line is a bit lossy and very long, i.e., there is no reflection: the waves along the MTL move only in $+z$-direction. Symmetric MTL geometry implies that the propagation modes are even and odd. Thus, the true voltages along the line can be written as [13]

$$\begin{pmatrix} V_1(z) \\ V_2(z) \end{pmatrix} = V_{\mathrm{m1}} \begin{pmatrix} 1 \\ 1 \end{pmatrix} e^{-j\beta_{\mathrm{m1}} z} + V_{\mathrm{m2}} \begin{pmatrix} 1 \\ -1 \end{pmatrix} e^{-j\beta_{\mathrm{m2}} z} \tag{14}$$

At the interface $z = 0$, one gets:

$$\begin{pmatrix} V_{\mathrm{m1}} \\ V_{\mathrm{m2}} \end{pmatrix} = \frac{1}{2} \begin{pmatrix} 1 & 1 \\ 1 & -1 \end{pmatrix} \begin{pmatrix} V_1(0) \\ V_2(0) \end{pmatrix} \tag{15}$$

So, the amplitudes for the even and odd mode, $V_{\mathrm{m1}}$ and $V_{\mathrm{m2}}$, can be computed from (15). If the excitation voltages correspond to even mode, $V_{\mathrm{m1}} \neq 0$ and $V_{\mathrm{m2}} = 0$. If the excitation is $(2 \;\; 0)^T$, $V_{\mathrm{m1}} = V_{\mathrm{m2}} = 1$, i.e., both even and odd mode start to propagate along the MTL. With inhomogeneous medium, like in Figure 1, it holds that $\beta_{\mathrm{m1}} \neq \beta_{\mathrm{m2}}$. In this case, there is coupling between the true conductor voltages. Namely, at the points along the line, where the phase-shift difference $(\beta_{\mathrm{m2}} - \beta_{\mathrm{m1}})z$ is an odd multiple of $\pi$, true voltage amplitudes are reversed to $(0 \;\; 2)^T$ from the original $(2 \;\; 0)^T$. Here, one may see a certain connection to the gyrotropic mode converter, where the phase-shift difference $(\beta^- - \beta^+)d$ causes mode conversion, and with certain lengths $d$ a total change from TM to TE is obtained (see paper [P3], formulas (14) and (15) ). The more there is difference between the $\beta$'s of the eigenwaves, the shorter distance is needed for total voltage reversal or total mode conversion.

## 3.3 On the computation of transmission-line parameters

In paper [P2] the needed TL parameters, i.e. the propagation factors and impedances for TM and TE modes, are computed analytically. On the contrary, in paper [P1] the TL parameters are computed numerically. The essential parameters are matrices $\overline{\overline{C}}$ and $\overline{\overline{L}}$, because using these one can solve the phase velocities $v_i$, the voltage eigenvectors $\overline{V}_i$, and currents $\overline{I}_i$, for quasi-TEM modes $i = 1...n$. Note that the modes are solved assuming a lossless MTL, i.e., the conductance matrix $\overline{\overline{G}}$ and the resistance matrix $\overline{\overline{R}}$ are assumed zero. Firstly, this kind of approach is practical, because the frequency-dependent eigenvalue equation

$$(j\omega\overline{\overline{C}} + \overline{\overline{G}}) \cdot (j\omega\overline{\overline{L}} + \overline{\overline{R}}) \cdot \overline{I} = \gamma^2 \, \overline{I} \, , \qquad \gamma = \alpha + j\beta, \tag{16}$$

simplifies to

$$\overline{\overline{C}} \cdot \overline{\overline{L}} \cdot \overline{I} = \frac{\beta^2}{\omega^2} \, \overline{I} = \frac{1}{v^2} \overline{I} \, , \tag{17}$$

which is frequency-independent eigenvalue equation. Secondly, this approximative approach is justified. In ceramic filters, the ceramic medium has $\tan\delta =$

[13] For simplicity, voltage eigenvectors are not normalised to unity here.

0.00005...0.0002, when frequency is around 1 GHz [31]. Imaginary part of the permittivity is thus very small, of order $10^{-4}$ compared to the real part. Thus, $\epsilon$ is assumed real, or $\overline{\overline{G}} = 0$, when solving the propagation modes. The dominant loss mechanism is the conductor losses. When solving the mode velocities, voltages, and currents, also these ohmic losses are neglected, i.e., $\overline{\overline{R}} = 0$. This approximation is justified, because in a ceramic filter, $r/\omega l$ is of order 0.005, where $r$ and $l$ are self resistance and inductance, respectively, of a cylindrical inner conductor (it has been assumed here that $f \sim 1$ GHz, $\sigma \sim 5 \cdot 10^7$ S/m, and conductor radius $\sim 0.5$ mm). However, slightly non-ideal conductors can be taken into account afterwards. This means that the attenuation factors $\alpha_i$ can be computed using the current distributions of the lossless MTL. Finally - note that the capacitance and inductance matrices, $\overline{\overline{C}}$ and $\overline{\overline{L}}$, are per-unit-length (PUL) quantities. The unit for $\overline{\overline{C}}$ is As/Vm=F/m and the unit for $\overline{\overline{L}}$ is Vs/Am=H/m.

### 3.3.1 Computing matrices $\overline{\overline{C}}$ and $\overline{\overline{L}}$

On the inner conductors of an MTL, the per-unit-length (PUL) charges $\overline{q}$, are related to conductor voltages $\overline{V}$ via equation

$$\overline{q} = \overline{\overline{C}} \cdot \overline{V} \tag{18}$$

On the other hand, for an MTL filled with air, it holds

$$\overline{\overline{L}} = \mu_0 \epsilon_0 \overline{\overline{C}}_0^{-1}, \tag{19}$$

where $\overline{\overline{C}}_0$ is the PUL capacitance matrix in case $\epsilon(x, y) = \epsilon_0$, i.e., the medium is homogeneous air. So usually, both $\overline{\overline{C}}$ and $\overline{\overline{L}}$ can be obtained via solving a capacitance matrix [14]. The procedure of capacitance computation utilises equation (18). Let index $k$ run from $1...n$, where $n$ is the number of inner conductors. For each $k$:

1. Set inner conductor voltages to $\overline{V}_k$. The outer conductor is in zero potential.
2. Using finite-difference method, solve 2-D static potential distribution $\phi_k(x, y)$.
3. From $\phi_k(x, y)$, the PUL charges on conductors, $\overline{q}_k$, are obtained by integrating the normal electric flux density $\mathbf{u}_n \cdot \mathbf{D}_k(x, y) = -\epsilon \mathbf{u}_n \cdot \nabla \phi_k(x, y)$ around each conductor. $\mathbf{u}_n$ is the unit normal vector for the integration path pointing away from the conductor. $\mathbf{u}_n$ and the integration path lie both in the plane that is perpendicular to the MTL axis ($z$-axis). In the FD program rectangle-shaped integration paths were used [15].

As a result, one gets vectors $\overline{q}_k$, which correspond to vectors $\overline{V}_k$. Using (18) as

$$\overline{q}_k = \overline{\overline{C}} \cdot \overline{V}_k, \quad k = 1...n, \tag{20}$$

[14] However, if the medium inside the MTL is also inhomogeneously magnetic, $\mu = \mu(x, y)$, inductance matrix $\overline{\overline{L}}$ can not be obtained via (19). Instead, separate 2-D magnetostatic problems have to be solved.

[15] Further, many integration paths were used around each conductor to monitor, whether different paths give the same value for the conductor charge (as it should be).

one obtains enough conditions to calculate $\overline{\overline{C}}$.

Here it is described shortly, how to obtain a static potential distribution for a MTL cross-sectional geometry, using 2-D FD method. In a region without free charges, Maxwell equation (3) has to hold with $\varrho = 0$, i.e., $\nabla \cdot \mathbf{D} = 0$. From this, using Gauss's theorem and assuming a 2-D case with a region surrounded by curve $C$, one gets

$$\oint_C \epsilon \nabla \phi(x, y) \cdot \mathbf{u}_n dc = 0 \tag{21}$$

From this, approximating normal derivatives on curve $C$ as difference quotients, one obtains an updating equation for potential (see Figure 10):

$$\phi_0 = \frac{\phi_1 + \phi_3}{4} + \frac{\epsilon_1 \phi_2 + \epsilon_2 \phi_4}{2(\epsilon_1 + \epsilon_2)} \tag{22}$$

If the potential point to be updated is not at a material interface, in that case

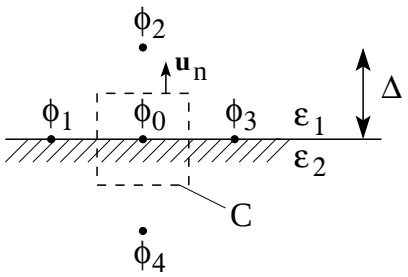


Figure 10: Potential $\phi_0$ can be approximated using the surrounding values.

$\phi_0 = (\phi_1 + \phi_2 + \phi_3 + \phi_4)/4$, i.e., simple average value. Of course, potentials on conductors (boundary conditions) are kept constant during updating process. Using (22) iteratively, the discrete potential distribution converges to its final state [16]. In practice, convergence speed is increased in two ways. Firstly, the density of the potential points is not constant during the iteration: iteration starts with lower density (higher value of $\Delta$). Secondly, a so-called relaxation parameter $F_R$ is used [32, pp. 24 –29]. Instead of (22), the potential is updated using equation

$$\phi_0^{m+1} = \phi_0^m + F_R \left( \phi_\Sigma^m - \phi_0^m \right), \quad \text{where} \quad \phi_\Sigma^m = \frac{\phi_1^m + \phi_3^m}{4} + \frac{\epsilon_1 \phi_2^m + \epsilon_2 \phi_4^m}{2(\epsilon_1 + \epsilon_2)} \ . \tag{23}$$

If $2 > F_R > 1$, convergence can be speeded up in a stable way. A good value seems to be between $F_R = 1.6...1.9$.

[16] Final state: the conductor charges do not remarkably change anymore as the iteration proceeds.

### 3.3.2 Solving the quasi-TEM modes

When $\overline{\overline{C}}$ and $\overline{\overline{L}}$ are known, the eigenvalue equation (see paper [P1])

$$\overline{\overline{C}} \cdot \overline{\overline{L}} \cdot \overline{I}_i = \frac{\beta_i^2}{\omega^2}\, \overline{I}_i = \frac{1}{v_i^2}\overline{I}_i \ , \qquad i = 1...n, \tag{24}$$

can be solved to obtain eigenvectors $\overline{I}_i$ and phase-velocities $v_i$. Vectors $\overline{I}_i$ can be normalised e.g. to unity. Within this thesis the MTL structures are such that the eigenvectors can be assumed real, i.e., $\overline{I}_i^* = \overline{I}_i$. $\overline{\overline{C}}$ and $\overline{\overline{L}}$ are real and symmetric. If the eigenvalues are distinct, i.e., there is no degenerate modes, eigenvectors can be chosen real [33, p.2092]. Define matrix $\overline{\overline{T}}_I$ so that it consists of column vectors $\overline{I}_i$, i.e., $\overline{\overline{T}}_I = [\overline{I}_1\ \overline{I}_2\ ...\ \overline{I}_n]$. If $\overline{\overline{T}}_V$ consists of column vectors $\overline{V}_i$, one may require that

$$\overline{\overline{T}}_V^T \cdot \overline{\overline{T}}_I = \overline{\overline{I}}, \tag{25}$$

where $\overline{\overline{I}}$ is the unit matrix. This means that the modes are power orthogonal, i.e., $\overline{V}_i^T \cdot \overline{I}_j = 0$ if $i \neq j$. The requirement (25) also forces that $\overline{V}_i^T \cdot \overline{I}_i = 1$, which causes that the true time-average propagating power is equal to $\frac{1}{2}\Re\{\sum_{i=1}^n V_{\mathrm{mi}} I_{\mathrm{mi}}^*\}$ [17]. So - if the norms of $\overline{I}_i$ are chosen, the eigenvectors $\overline{V}_i$ are automatically determined through (25). This subject, decoupling the MTL equations, is extensively discussed in [34], [26], and [33].

Finally, let us briefly discuss the accuracy of various numerically computed parameters and their effect on the frequency response. Assume an MTL having symmetrical cross-sectional geometry with three ($n = 3$) cylindrical conductors so that the medium inside is inhomogeneous (like the MTL in Figure 1). The conductors are given indices 1,2, and 3, from left to right. Due to the symmetry of the MTL, $C_{11} = C_{33}$ and $C_{23} = C_{12}$. Also, $L_{11} = L_{33}$ and $L_{23} = L_{12}$. It is realistic to assume the following relative errors in the elements of the $\overline{\overline{C}}$ and $\overline{\overline{L}}$ matrices: $\delta C_{11}/C_{11} = 0.01$, $\delta C_{22}/C_{22} = 0.01$, $\delta C_{12}/C_{12} = 0.02$, $\delta C_{13}/C_{13} = 0.06$, and, $\delta L_{11}/L_{11} = 0.01$, $\delta L_{22}/L_{22} = 0.01$, $\delta L_{12}/L_{12} = 0.01$, $\delta L_{13}/L_{13} = 0.02$. These estimates are based on an earlier comparison: the results of the FD-method-based $\overline{\overline{C}}, \overline{\overline{L}}$-computation routine have been compared to the results obtained with a commercial BEM program (BEM = Boundary Element Method). Assuming the above-mentioned accuracy in the elements of $\overline{\overline{C}}$ and $\overline{\overline{L}}$ matrices, the error in eigenvector elements and in the phase velocities of the modes is around 1 %. However, in practice, the errors can be even smaller. To illuminate the reason for this, assume simply an inhomogeneous two-conductor TL having distributed parameters $C$ and $L$. Phase velocity is $1/\sqrt{CL} = 1/\sqrt{CC_0^{-1}\mu_0\epsilon_0}$. Now – $C$ and $C_0$ are computed numerically using the *same* FD-method routine. If *both* computed capacitance values are a bit too high, the error in phase velocity can be very small. It is evident that the accuracy in phase velocities is same as the accuracy of the quasi-TEM resonance frequencies.

[17] In an MTL, time-average true power flow is the real part of

$$P = \frac{1}{2}\overline{V}^T(z) \cdot \overline{I}^*(z) = \frac{1}{2}(\sum_{i=1}^n V_{\mathrm{mi}} e^{-j\beta_i z}\overline{V}_i^T) \cdot (\sum_{i=1}^n I_{\mathrm{mi}} e^{-j\beta_i z}\overline{I}_i)^* = \frac{1}{2}\sum_{i=1}^n V_{\mathrm{mi}} I_{\mathrm{mi}}^* \overline{V}_i^T \cdot \overline{I}_i$$

If now requiring $\overline{V}_i^T \cdot \overline{I}_i = 1$, $P = \frac{1}{2}\sum_{i=1}^n V_{\mathrm{mi}} I_{\mathrm{mi}}^*$.

### 3.3.3 Attenuation factors due to conductor losses

If the conductors are non-ideal, electromagnetic wave is attenuated exponentially as it propagates along the MTL. Electric field for the propagation mode $i$ can be written as

$$\mathbf{E}_i(x,y,z) = \mathbf{E}_i(x,y)e^{-j\beta_i z}e^{-\alpha_i z}. \tag{26}$$

Solving attenuation factor $\alpha_i$ requires computing the per-unit-length loss power $P_{l,i}$ and the propagating power $P_{p,i}$, i.e.,

$$\alpha_i = \frac{P_{l,i}}{2P_{p,i}}. \tag{27}$$

At the surface of a non-ideal conductor, the time-average power-flow density into the conductor is

$$S_{loss} = \frac{1}{2}\Re\{\mathbf{E}\times\mathbf{H}^*\}\cdot(-\mathbf{u}_n) = \frac{1}{2}\Re\{-\mathbf{u}_n\times\mathbf{E}\cdot\mathbf{H}^*\}, \tag{28}$$

where $\mathbf{u}_n$ is the surface normal pointing away from the conductor. With very good conductivity $\sigma$, the relation between the $\mathbf{E}$ and $\mathbf{H}$, using wave impedance, becomes $-\mathbf{u}_n\times\mathbf{E} = \sqrt{\mu_0/(\sigma/j\omega)}\,\mathbf{H}$. Thus, from (28) one gets

$$S_{loss} = \frac{1}{2}\Re\left\{\sqrt{\frac{\omega\mu_0}{\sigma}}\,\frac{1+j}{\sqrt{2}}\,H^2\right\} = \frac{1}{2}\sqrt{\frac{\omega\mu_0}{2\sigma}}\,H^2 = \frac{1}{2}R_sH^2, \tag{29}$$

where $R_s$ is the surface resistance and $H$ is the magnetic field strength at the surface. For a quasi-TEM mode $i$, the magnetic field is

$$\mathbf{H}_{t,i}(x,y) = \mathbf{u}_z\times\frac{\mathbf{E}_{t,i,0}(x,y)}{\eta_i} = -\mathbf{u}_z\times\frac{\nabla\phi_{i,0}(x,y)}{\eta_i}, \tag{30}$$

where $t$ stands for 'transverse', $\phi_{i,0}(x,y)$ is the potential distribution in case of homogeneous medium and $\eta_i$ is the effective wave impedance of mode $i$. Using (30) in (29), at a conductor surface one gets

$$S_{loss,i} = \frac{R_s}{2\eta_i^2}\left|\frac{d\phi_{i,0}(x,y)}{dn}\right|^2. \tag{31}$$

The total per-unit-length loss power of mode $i$, $P_{l,i}$, is obtained by integrating $S_{loss,i}$ over the circumference of each conductor. Thus

$$P_{l,i} = \frac{R_s}{2\eta_i^2}\sum_{j=0}^{n}\oint_{c_j}\left|\frac{d\phi_{i,0}(x,y)}{dn}\right|^2 dc, \tag{32}$$

which is the same as formula (37) in paper [P1].

One way to compute the propagating power of mode $i$ is to use circuit quantities:

$$P_{p,i} = \frac{\overline{V}_i^T\cdot(\overline{\overline{Z}}_c^{-1}\cdot\overline{V}_i)}{2}, \tag{33}$$

where $\overline{\overline{Z}}_c$ is the characteristic impedance matrix, relating the voltages and currents of a propagating wave. $\overline{\overline{Z}}_c$ depends on the MTL cross-sectional geometry and media. Different useful formulas for $\overline{\overline{Z}}_c$ can be derived [34], for example

$$\overline{\overline{Z}}_c = \frac{1}{\omega}\overline{\overline{C}}^{-1} \cdot \overline{\overline{T}}_I \cdot \overline{\overline{\beta}} \cdot \overline{\overline{T}}_I^{-1} = \overline{\overline{C}}^{-1} \cdot \overline{\overline{T}}_I \cdot \overline{\overline{\Lambda}} \cdot \overline{\overline{T}}_I^{-1}, \tag{34}$$

where $\overline{\overline{\Lambda}}$ is a diagonal matrix so that $\overline{\overline{\Lambda}}^2$ has eigenvalues $\frac{1}{v_i^2}$ in its diagonal. So - using (27), (32), and (33) one obtains the attenuation factors.

Loss power can be also obtained via resistance matrix $\overline{\overline{R}}$, which often gives usable results quickly, because $\phi_{i,0}(x,y)$ distributions need not to be computed. The PUL loss power of mode $i$ can be approximated as (see paper [P1] for details)

$$P_{l,i} = \frac{1}{2}\overline{I}_i^T \cdot \overline{\overline{R}} \cdot \overline{I}_i, \qquad \overline{I}_i = \overline{\overline{Z}}_c^{-1} \cdot \overline{V}_i \tag{35}$$

From (27), (32), and (33), it is seen that all the quasi-TEM attenuation factors depend on $R_s \propto \sqrt{f/\sigma}$. Thus, one can compute $\alpha_i$'s using e.g. $f = 1$ GHz and $\sigma = 6.17 \cdot 10^7$ S/m (silver) [35]. If the frequency of analysis is e.g. doubled, all the $\alpha_i$'s should be multiplied by $\sqrt{2}$.

## 3.4 FDTD shortly

The dynamical behaviour of electromagnetic fields in space and time can be simulated using FDTD (Finite-Difference Time-Domain), which essentially means solving Maxwell's equations approximately in discretised space and time coordinates. The usual FDTD scheme assumes a so-called Yee's cell [36], where the discrete space-time points of electric field are shifted from the points of the magnetic field, i.e., the E-grid is translated away from the H-grid by vector $\frac{1}{2}(\Delta x, \Delta y, \Delta z, \Delta t)$. FDTD is a leap-frog algorithm: as the time-stepping propagates, electric and magnetic fields are updated alternately. For example, for $E_z$ component the "normal" updating equation is

$$\begin{aligned} E_z(x,y,z,t+\Delta t) &= \tfrac{2\epsilon_z - \sigma\Delta t}{2\epsilon_z + \sigma\Delta t} E_z(x,y,z,t) \\ &+ \tfrac{2\Delta t}{(2\epsilon_z+\sigma\Delta t)\Delta x}\left[H_y(x+\tfrac{\Delta x}{2},y,z,t+\tfrac{\Delta t}{2}) - H_y(x-\tfrac{\Delta x}{2},y,z,t+\tfrac{\Delta t}{2})\right] \\ &+ \tfrac{2\Delta t}{(2\epsilon_z+\sigma\Delta t)\Delta y}\left[H_x(x,y-\tfrac{\Delta y}{2},z,t+\tfrac{\Delta t}{2}) - H_x(x,y+\tfrac{\Delta y}{2},z,t+\tfrac{\Delta t}{2})\right], \end{aligned} \tag{36}$$

where $\epsilon_z$ is permittivity in $z$-direction, $\sigma$ is conductivity of the medium, $\Delta x$ and $\Delta y$ are cell dimensions, and $\Delta t$ is the time-step length. For other field components equations are similar. The updating equations can be derived from Maxwell's equations by approximating time and spatial derivatives by difference quotients. For example,

$$\begin{aligned} &\tfrac{\partial}{\partial x} H_y(x,y,z,t+\tfrac{\Delta t}{2}) \approx \\ &\tfrac{1}{\Delta x}\left[H_y(x+\tfrac{\Delta x}{2},y,z,t+\tfrac{\Delta t}{2}) - H_y(x-\tfrac{\Delta x}{2},y,z,t+\tfrac{\Delta t}{2})\right]. \end{aligned}$$

In addition to (36), many other kind of updating rules are also needed, like for the absorbing boundary condition (ABC) [37], or for curved medium interfaces [38]. FDTD has been studied widely during the last ten years [39].

### 3.5 Block-by-block circuit model or all at once?

If something can be modelled using circuit theory, i.e. by using transmission lines and discrete components, the modelling can be really fast. The problem is that first, one has to solve the circuit parameter values, such as the TL propagation constants, characteristic impedances, and possibly some discrete component values e.g. for a waveguide discontinuity. In practice, circuit simulation does not take time at all, but parameter value extraction of a physical structure may take a long time.

Earlier it was already discussed that many of the studied structures can be sensibly modelled by transmission lines. The investigated PBG structures are an exception. Because they are complex and non-uniform, involving e.g. tapered bends, very much different circuit parameter values should be computed [18]. Parameters should be frequency dependent. Also, if many modes can propagate, one should know the TL parameters for different modes. Further, at discontinuities such as bends or tapering sections, modes are coupled, i.e., it might be necessary to compute the coupling parameters too. The fact that the bend operation is sensitive to the hole positions, complicates the situation further. For these reasons, instead of the parametric block-by-block approach, the PBG-WG components have been modelled as the whole structure at once.

## 4 Summary of publications

### [P1]: Application of multiconductor transmission-line theory to combline filter design

Paper [P1] proposes an efficient design method for combline filters having inhomogeneous medium. The frequency is assumed small enough so that the filter operation is mainly determined by quasi-TEM modes. It follows that the filter can be approximated as multiple multiconductor transmission lines (MTL) cascaded. Thus, a circuit simulator can be used along the design process. Although numerical field computation is needed to obtain the MTL-parameter values (matrices $\overline{\overline{C}}$ and $\overline{\overline{L}}$), the mean simulation time is short. The paper starts with a discussion of quasi-TEM and MTL theory. Thereafter, computation of MTL parameters numerically is considered. Next, the filter design process using circuit simulator is discussed. Finally, a numerical example is given. In the example, $\overline{\overline{C}}$ and $\overline{\overline{L}}$ are computed for two MTL sections, which as cascaded form the combline-filter structure. As $\overline{\overline{C}}$ and $\overline{\overline{L}}$ matrices have been computed, the voltages, currents, and the phase velocities of quasi-TEM modes can be solved. Knowing the mode parameters, the system of cascaded MTL's (filter) is modelled using a circuit simulator. As a result, it is observed that a 3-D FEM software and circuit simulator give about the same results for the frequency

[18] However, if the PBG component is simply a uniform monomode periodic waveguide, the essential parameters are the propagation factor $\beta(f)$ and the attenuation factor $\alpha(f)$ of the lowest mode. Approximations for these curves can be obtained e.g. via a single FDTD simulation and Fourier transform of the fields at certain observation planes [40]. Dispersion curve $\beta(f)$ is computed using the phase difference between two observation planes, $\alpha(f)$ is obtained from the propagating-power difference.

response $|S_{21}(f)|$ of the filter. However, by using a circuit simulator assisted by numerical capacitance computation, the response is obtained in e.g. 10 seconds, while with 3-D FEM the needed time is 10 minutes.

## [P2]: Fields in anisotropic hard-surface waveguide with application to polarisation transformer

In paper [P2] electromagnetic fields inside a circular waveguide with axial corrugation are studied. The corrugation is assumed such that the boundary condition is equal to a hard surface: at $\rho = a$, axial fields $H_z = E_z = 0$. The waveguide is filled with uniaxial anisotropic material. The treatment is analytical, assuming time-harmonic fields ($\propto e^{j\omega t}$) and $z$ dependency as $e^{\pm j\beta z}$.

Decomposing fields to transverse and longitudinal parts, $\mathbf{E} = \mathbf{e} + E_z\mathbf{u}_z$ and $\mathbf{H} = \mathbf{h} + H_z\mathbf{u}_z$, and using these with Maxwell's equations and with constitutive relations, Helmholtz equations

$$\begin{aligned}
[\nabla_t^2 + (\omega^2\epsilon_t\mu_t - \beta^{TM\,2})\frac{\epsilon_z}{\epsilon_t}]E_z &= 0 \\
[\nabla_t^2 + (\omega^2\epsilon_t\mu_t - \beta^{TE\,2})\frac{\mu_z}{\mu_t}]H_z &= 0
\end{aligned}$$

are obtained (for briefness, these were not shown in the article). Hard surface does not couple $E_z$ and $H_z$ at all. Thus, the eigenfields in an anisotropic hard-surface waveguide are TM and TE fields, for which it holds $\mathbf{e}^{TM} \perp \mathbf{e}^{TE}$, and which are travelling with different propagation factors, $\beta^{TM} \neq \beta^{TE}$. The polarisation transformation is based on this difference: as the total field $\mathbf{e} = \mathbf{e}^{TM} + \mathbf{e}^{TE}$ travels along the anisotropic WG, the relative phase between $\mathbf{e}^{TM}$ and $\mathbf{e}^{TE}$ is changed.

The paper starts with the analysis of the propagation modes in an anisotropic hard-surface waveguide (HS-WG). Knowing the mode propagation factors and impedances, a transmission-line model can be used in the reflection-transmission analysis. For a HS-WG chain structure of type isotropic-anisotropic-isotropic, the reflection and transmission coefficients are obtained for TM and TE mode. Thus, for example, transmitted longitudinal field amplitudes are $E_n^t = T^{TM}E_n$ and $H_n^t = T^{TE}H_n$. Using these with equations (7) and (8), one obtains the total transmitted field $\mathbf{e}^t = \mathbf{e}^{t,TM} + \mathbf{e}^{t,TE}$. Applying helicity vector $\mathbf{p}$ [41] as

$$\mathbf{p} = \frac{\mathbf{e}^t \times \mathbf{e}^{t*}}{j\mathbf{e}^t \cdot \mathbf{e}^{t*}} \ ,$$

the polarisation state of the transmitted field is obtained. The paper is ended with application examples. For example, a polarisation transformation from linear to elliptical is considered. Power-transmission and helicity curves are shown for a well-matched transformer and for a mismatched transformer. In the well-matched case the power transmission is close to 100 % and linear polarisation is very closely changed to circular polarisation. (Note that in the original article the curves have been drawn incorrectly, see Errata.)

## [P3]: Mode transformer for hard-surface waveguides

In paper [P3] a circular hard-surface waveguide is filled with gyrotropic material, e.g. magnetoplasma or ferrite. In the paper the focus is on ferrite filling. It is assumed that the material is only slightly anisotropic and gyrotropic, i.e., $\mu_t \approx \mu_z$ and $\mu_g/\mu_t \approx 0$. Via analytical treatment, assuming time-harmonic fields, mode-transformation effect is considered, for example, from $\mathrm{TM}_z$ to $\mathrm{TE}_z$ mode. The eigenwaves in the gyrotropic waveguide are elliptically polarised hybrid-mode fields, which propagate with slightly different propagation factors. This difference in propagation factors causes the mode transformation, as the waves propagate through the gyrotropic waveguide section.

The eigenfields and the corresponding propagation factors for the gyrotropic HS-WG must be solved first. Assuming $z$ dependency $e^{-j\beta z}$ and $\mu_g/\mu_t$ small, decomposing fields as $\mathbf{E} = \mathbf{e}+E_z\mathbf{u}_z$ and $\mathbf{H} = \mathbf{h}+H_z\mathbf{u}_z$, and using these with Maxwell's equations and with constitutive relations, Helmholtz equations are obtained. Two eigenfield solutions can be identified and named as plus and minus waves. These are elliptically polarised hybrid-mode fields. Using the HS boundary condition, cut-off wavenumbers are obtained. Thereafter, assuming $\mu_g/\mu_t$ small, approximative values for propagation factors $\beta^{\pm}$ are solved.

Next, in the gyrotropic section, the total longitudinal electric and magnetic fields are written as a sum of the plus and minus waves. Assuming a good matching at the isotropic-gyrotropic interface, a TM-TE transformer is considered. In this simple reflectionless case, formulas (14) and (15) describe the mode transformation along the gyrotropic section. At $z = 0$, amplitude of $E_z \neq 0$, and $H_z = 0$ in the whole WG cross-section (TM). But at $z = d = \frac{\pi\mu}{\mu_g k}$, $E_z = 0$, and amplitude of $H_z \neq 0$ (TE). The incident $E_z(\rho, \varphi)$ has thus been replaced by $H_z(\rho, \varphi)$ so that these fields have the same $(\rho, \varphi)$ dependency. Thus, the field configuration before the gyrotropic WG satisfies the PEC boundary condition, and after the gyrotropic WG the field satisfies the PMC boundary condition. Because the relation between the transverse fields $\mathbf{e}$ and $\mathbf{h}$ is changed, the gyrotropic HS-WG can be also seen as an impedance transformer, i.e., as a matching element between two different kind of circular waveguides. One application is a matching element between a metal-wall waveguide and an open dielectric waveguide or antenna.

## [P4]: Analysis of finite-length gyrotropic hard-surface waveguide

In paper [P4] the authors continue with the research of gyrotropic hard-surface waveguide. The effect of gyrotropy is taken into account exactly, i.e., no approximation of small gyrotropy or small anisotropy is made. Also, in the mode-transformer structure, reflections are taken into account. Reflection and transmission formulas are derived for a structure of type isotropic-gyrotropic-isotropic in a general case. Mode-transformer examples are given.

As in the previous paper, also in this paper the analysis starts with the search of the eigenfields and the corresponding propagation factors in a gyrotropic HS-WG. It is already known from [P3] that the eigenfields are hybrid, i.e., $E_z$ and $H_z$ are coupled. This is seen e.g. from Helmholtz equation (18) of the present paper.

As the eigenmodes and propagation factors are known for isotropic and gyrotropic HS-WG sections, one can start studying the interfaces isotropic-gyrotropic (IG) and gyrotropic-isotropic (GI). So, in the isotropic WG the basis is TM and TE modes and in the gyrotropic WG the basis is + and − waves. By requiring the continuity of the transverse fields **e** and **h** at the interfaces, the reflection and transmission matrices are obtained for the IG and GI interfaces. For example, by using the matrix $\overline{\overline{T}}_{IG}$, the transmitted + and − wave amplitudes are obtained, if the incident TM and TE amplitudes are known.

Now, having the model for IG and GI interface, a model for a finite-length gyrotropic WG (mode transformer) can be constructed. Using this, the transmission and reflection of TM and TE modes will be obtained. The paper is ended with mode-transformer examples. In the first example, a well-matched small-gyrotropy case is considered. With properly chosen length of the ferrite-filled WG, the incident TM mode is entirely transformed to TE. In the second example, the ferrite-filled section is between two air-filled waveguides. The reflected power in this case is very high in average, but still at some frequencies, the incident TM power is transformed to transmitted TE power. Changing the bias magnetic flux density $B_o$ shifts the transmission spectrum. Hence, for example, one can tune the transmission peak to the operation frequency range of the HS boundary.

## [P5]: Studying 120° PBG waveguide bend using FDTD

Photonic-bandgap-waveguide (PBG-WG) structures are considered. The WG's are based entirely on linear dielectric media. Analysis is based on numerical field computation by FDTD and post-processing of the field data. A 120° PBG-WG bend is investigated as an example. Power-transmission results are given. Various issues related to simulation arrangements and PBG-WG-component design are discussed.

After the introduction, the analysis method is discussed. Shortly, the method resembles a "virtual measurement setup". There must be a source i.e. a field excitation, for which time and spatial dependency is properly chosen. The behaviour of EM fields is governed by Maxwell's equations, which are solved using FDTD. Also, there must be observation surfaces, on which time-dependent fields are sampled and stored to hard disk for post-processing. Post-processing involves interpolation and Fourier transform of the fields, power-flow computation in time and frequency domains, and computation of reflection and transmission spectra. At the end of the analysis section, the method is shown to give reasonable results.

Next section describes results obtained for a 120° PBG-WG bend. Relative hole size $d/a = 0.76$ is kept constant. Quasi-$\mathrm{TE}_z$ polarisation has been assumed (electric field effectively perpendicular to the axes of the air cylinders). The relevance of optimising the bend geometry is shown. It becomes clear that seemingly small changes in the hole configuration can change component operation dramatically. Also, the effect of finite PBG-plate thickness is shown: as can be expected, the radiation losses drop the transmission level, and the decrease of the effective refraction index slightly upshifts the spectrum in frequency.

Finally, design and optimisation issues are discussed. Optimisation requires obtaining reasonable modelling results in reasonable time. In the paper it is checked how much the transmission spectrum depends on the time-window length and on

the FDTD cell size. It is observed that usable results are obtained even with quite modest time-window lengths and with a cell size $\Delta = a/10$, where $a$ is the lattice constant. This suggests that the method really suits for PBG-WG-structure optimisation. However, it is also remarked that special slow-convergence regions may exist in spectra, and that there may be structures with special frequencies, for which the power flow can be very sensitive to the cell size, and to the relative hole size $d/a$.

## [P6]: Fabrication of photonic crystal waveguide elements on SOI

The paper reports on fabrication of photonic-crystal-waveguide elements on SOI (silicon-on-insulator). As in the previous paper, the photonic crystals have a triangular lattice structure with cylindrical air columns. The paper focuses on the fabrication issues, problems encountered, and possible solutions. The test structures, 60° and 120° bends, and the taper, were designed using the modelling methods described in paper [P5].

After the introduction, design and modelling issues are discussed. Thereafter, the fabrication process is explained. Finally, fabrication results are reported. Top-view figures of regular photonic crystals and waveguide elements are shown. Also, sideview-profile figures are shown. From these, the etch profile can be examined.

The author wishes to make some clarifications about the modelling and design process. The bends and the taper were designed with $d/a = 0.76$. The value 0.76 was chosen using fuzzy logic, keeping various things in mind. Firstly, $d/a$ should not be too high, because

- increasing hole diameter $d$ tends to increase radiation losses
- high $d/a$ value makes the walls between the holes thin. This may cause trouble in fabrication. It was decided that wall thickness should be roughly $\geq 100$ nm.

Secondly, $d/a$ should not be too small.

- With too small $d/a$ there is no band gap at all. $d/a$ should be at least about 0.4 to have a TE band gap [16, p. 125], [24].
- Considering fabrication, too small $d/a$ value is not practical.
- As $d/a$ is increased, so is the band-gap width. Wider band gap makes the PBG lattice a better reflector.
- With high $d/a$ value there is potential for a common TE and TM band gap.

At the time when the $d/a$ value was decided, wide band gap (stop band) was preferred. The minimisation of radiation losses was not considered crucial at that time. After deciding that $d/a = 0.76$, the structures were designed. Design process involved testing different hole configurations. The fuzzy goal was, for example, to have a good power transmission for a bend so that the hole configuration is very simple, i.e., as regular as possible. The bend components and the taper section were designed to be compatible with each other. The components have maximum

transmission at the same frequency and the components can be directly cascaded. Finally, it should be understood that the optimum hole configuration depends on $d/a$. Changing the $d/a$ value, e.g. from 0.76 to 0.6, implies redesign of the hole configuration.

As the discussion of the paper shows, the fabrication of real PBG-WG structures for infrared regime is a demanding challenge. It has been assumed in the paper that $\lambda_0 \approx 1.5\mu$m. In the paper, SEM (scanning electron microscopy) figures are shown. For example, Figures 6 and 7 show sideview profiles of the air columns after silicon etching. Etch profile is vertical and often quite smooth. Top-view Figure 8 shows the designed waveguide elements after oxide and silicon etching. Hole positioning in the fabrication process seems to be working well. Some unwanted variation in the hole size has been caused by the so-called proximity effect. In general, the fabrication results are promising, although some non-idealities are clearly apparent.

However, it should be remembered that seemingly small nonidealities in the structure may have a strong effect on the device operation. For example, as was seen in the example of paper [P5], perturbing the hole positions changed totally the transmission spectrum of the 120° bend. A seemingly small perturbation may be electromagnetically remarkable. Although this may make the fabrication of certain components challenging, with e.g. sensor components this sensitivity is a benefit.

# References


[1] T. Uusitupa, J. Loukkola. On the modelling of ceramic combline RF-filter. In *Proceedings of the 27th European Microwave Conference, Jerusalem, Israel*, pages 1092–1097, Sep 1997.

[2] A.J. Viitanen, T.M. Uusitupa. Polarisation properties of fields propagating in anisotropic hard surface waveguide. In *Proceedings of the 11th Conference and Exhibition on Microwaves, Radio Communication and Electromagnetic Compatibility, MIOP, Stuttgart, Germany*, pages 49–54, May 2001.

[3] T. Uusitupa, K. Kärkkäinen. Modelling photonic bandgap structures using FDTD. In *Proceedings of Bianisotropics 2000, Lisbon, Portugal*, pages 285 – 288, Sep 2000.

[4] I.V. Lindell, A.H. Sihvola, S.A. Tretyakov, and A.J. Viitanen. *Electromagnetic waves in chiral and bi-isotropic media*. Artech House, 1994.

[5] I. V. Lindell. *Aaltojohtoteoria*. Otatieto, 1997. (in Finnish).

[6] R. F. Harrington. *Time-Harmonic Electromagnetic Fields*. John Wiley & Sons, Inc., 2001. An IEEE Press Classic Reissue.

[7] R. E. Collin. *Field Theory of Guided Waves*. IEEE Press, 2nd edition, 1991.

[8] S. Ramo, J. R. Whinnery, and T. van Duzer. *Fields and Waves in Communication Electronics*. John Wiley & Sons, Inc., 2nd edition, 1984.

[9] S. K. Koul. *Millimeter Wave and Optical Dielectric Integrated Guides and Circuits*. John Wiley & Sons, Inc., 1997.

[10] T. Rozzi, M. Mongiardo. *Open electromagnetic waveguides*, volume 43 of *IEE Electromagnetic waves series*. The Institution of Electrical Engineers, 1997.

[11] I.V. Lindell. *Radioaaltojen eteneminen*. Otatieto, 4th edition, 1996. (in Finnish).

[12] I. V. Lindell. On the quasi-TEM modes in inhomogeneous multiconductor transmission lines. *IEEE Trans. Microwave Theory Tech.*, 29(8):812 – 817, Aug 1981.

[13] P.J.B. Clarricoats, A.D. Olver. *Corrugated Horns for Microwave Antennas*. Stevenage: Peregrinus, 1984.

[14] P.-S. Kildal. Artificially soft and hard surfaces in electromagnetics. *IEEE Trans. Antennas Propagat.*, 38(10):1537–1544, Oct 1990.

[15] S.F. Mahmoud. *Electromagnetic Waveguides, Theory and Applications*, volume 32 of *IEE Electromagnetic waves series*. Peter Peregrinus Ltd., 1991.

[16] J. D. Joannopoulos, R. D. Meade, and J. N. Winn. *Photonic Crystals, Molding the Flow of Light*. Princeton University Press, 1995.

[17] R. Gonzalo, P. de Maagt, and M. Sorolla. Enhanced patch-antenna performance by suppressing surface waves using photonic-bandgap substrates. *IEEE Trans. Microwave Theory Tech.*, 47(11):2131–2138, Nov 1999.

[18] F. Falcone et al. Compact photonic bandgap microstrip structures. *Microwave and Optical Technology Letters*, 23(4):233 – 236, Nov 1999.

[19] E. Yablonovitch. Photonic band-gap structures. *J. Opt. Soc. Am. B*, 10(2):283 – 295, Feb 1993.

[20] S.E. Barkou, J. Broeng, and A. Bjarklev. Silica-air photonic crystal fiber design that permits waveguiding by a true photonic bandgap effect. *Optics Letters*, 24(1):46 – 48, Jan 1999.

[21] A. Mekis et al. High transmission through sharp bends in photonic crystal waveguides. *Phys. Rev. Lett.*, 77(18):3787–3790, Oct 1996.

[22] I. El-Kady, M. M. Sigalas, R. Biswas, and K.M. Ho. Dielectric waveguides in two-dimensional photonic bandgap materials. *IEEE Journal of Lightwave Technology*, 17(11):2042 – 2049, Nov 1999.

[23] B. D'Urso et al. Modal reflectivity in finite-depth two-dimensional photonic-crystal microcavities. *J. Opt. Soc. Am. B*, 15(3):1155 – 1159, Mar 1998.

[24] M. Allen. Gap maps for photonic crystals. Report 412, Helsinki University of Technology / Electromagnetics Laboratory, Aug 2003.

[25] T. Uusitupa. Design of a dual-mode filter using FDTD. In *Sähkömagnetiikka 99, The 9th Finnish Electromagnetics Meeting, Espoo*, pages 36–37, Aug 1999.

[26] C.R. Paul. *Analysis of Multiconductor Transmission Lines.* John Wiley & Sons, Inc., 1994.

[27] D.K. Cheng. *Field and Wave Electromagnetics.* Addison-Wesley, 2nd edition, 1991.

[28] A. Lehto, A. Räisänen. *RF- ja mikroaaltotekniikka.* Otatieto, 1994. (in Finnish).

[29] T. C. Edwards. *Foundations for Microstrip Circuit Design.* John Wiley & Sons, Inc., 2nd edition, 1992.

[30] R. K. Hoffman. *Handbook of Microwave Integrated Circuits.* Artech House, Inc., 1987.

[31] J. Loukkola. Keraamisuodattimen mallitus APLAC-piirisimulaattori-ympäristössä. Master's thesis, Oulun yliopisto, sähkötekniikan osasto, 1993. (in Finnish).

[32] R. C. Booton. *Computational Methods for Electromagnetics and Microwaves.* John Wiley & Sons, Inc., 1992.

[33] G-T Lei, G-W Pan, and B.K. Gilbert. Examination, clarification, and simplification of modal decoupling method for multiconductor transmission lines. *IEEE Trans. Microwave Theory Tech.*, 43(9):2090–2100, Sep 1995.

[34] C.R. Paul. Decoupling the multiconductor transmission line equations. *IEEE Trans. Microwave Theory Tech.*, 44:1429–1440, Aug 1996.

[35] K. Nikoskinen. *Sähkömagnetiikan kaavoja*. Otatieto, 1992. (in Finnish).

[36] K.S. Yee. Numerical solution of initial boundary value problems involving Maxwell's equations in isotropic media. *IEEE Trans. Antennas and Propagation*, 14(3):302 – 307, 1966.

[37] A. Taflove, S.C. Hagness. *Computational Electrodynamics, The Finite Difference Time Domain Method*. Artech House, 2nd edition, 2000.

[38] K. Kärkkäinen, A. Sihvola, and K. Nikoskinen. Analysis of a three-dimensional dielectric mixture with finite difference method. *IEEE Transactions on Geoscience and Remote Sensing*, 39(5):1013 – 1018, May 2001.

[39] http://www.fdtd.org.

[40] T.M. Uusitupa. Studying straight PBG waveguides using FDTD. Report 393, Helsinki University of Technology / Electromagnetics Laboratory, May 2002.

[41] I.V. Lindell. *Methods for electromagnetic field analysis*, volume 30 of *Oxford engineering science series*. Oxford University Press, 1992.

413. H. Kettunen, J. Sarvas: Computer program package for electromagnetic field computing with spherical vector wave functions, September 2003.

414. J. Avelin: Polarizability analysis of canonical dielectric and bi-anisotropic scatterers, September 2003.

415. A. Sihvola, J. Venermo, P. Ylä-Oijala: Dielectric response of matter with cubic, circular-cylindrical, and spherical microstructure, October 2003.

416. I.V. Lindell, K.H. Wallén: Differential-form electromagnetics and bi-anisotropic Q-media, November 2003.

417. S. Järvenpää, P. Ylä-Oijala: GMRES-FFT method for acoustic volume integral equation, November 2003.

418. S. Järvenpää, P. Ylä-Oijala: Hybrid boundary element-finite element method for impedance boundary value problems of Helmholtz equation, November 2003.

419. P. Ylä-Oijala, M. Taskinen, J. Sarvas: General surface integral equation method for composite metallic and dielectric structures, December 2003.

420. J.J. Hänninen, I.V. Lindell, K.I. Nikoskinen: Electrostatic image theory for an anisotropic boundary of an anisotropic half-space, December 2003.

421. I.V. Lindell, K.H. Wallén: Generalized Q-media and field decomposition in differential-form approach, December 2003.

422. H. Wallén, A. Sihvola: Polarizability of conducting sphere-doublets using series of images, January 2004.

423. A. Sihvola (editor): Electromagnetics Laboratory Annual Report 2003, February 2004.

424. J. Venermo, A. Sihvola: Electric polarizability of circular cylinder, February 2004.

425. A. Sihvola: Metamaterials and depolarization factors, February 2004.

426. T. Uusitupa: Studying electromagnetic wave-guiding and resonating devices, February 2004.

ISBN 951-22-7001-3
ISSN 1456-632X
Picaset Oy, Helsinki 2004